Modeling heat transfer in the vegetation-soil continuum

by

Rik Aulbers

to obtain the degree of Master of Science
at the Delft University of Technology,
to be defended publicly on Wednesday June 16, 2021 at 3:30 PM.

Student number:	4455223	
Project duration:	September 1, 2020 – June 16, 2021	
Supervisors:	Prof. dr. ir. B. J. H. Van de Wiel,	TU Delft
	Dr. ir. M.-C. ten Veldhuis,	TU Delft
	Dr. ir. S. van der Linden,	TU Delft
	Ir. J. Boekee	TU Delft

An electronic version of this thesis is available at `http://repository.tudelft.nl/`.

TU Delft

Abstract

This thesis contributes to the scientific underpinning of the battle against fruit frost. Fruit frost is the freezing damage to blossoms when in the growing season the night temperature drops below 0°C. This results in damaged or undeveloped fruits, and a yield loss for the fruit farmer. Several techniques against fruit frost have been developed, including sprinkling and wind machines, often in combination with meteorological models, for example, to predict air temperature. However, the contribution of heat exchange with the soil to moderate orchard temperatures is often not included. In this thesis, this heat transfer is investigated, as an increase of heat transfer from the soil to the orchard during the night is a potential remedy against fruit frost. The research is based on measurements for soil temperature, soil heat flux, and soil moisture from two locations (1. Haarweg (Gelderland), The Netherlands 2. Bushland (Texas), The U.S.A.). First, a numerical model is developed to calculate the temperature and soil heat flux profiles for a soil layer. The results are compared to the results of an already developed analytical model. Second, the thermal parameters, that are of influence on the heat transfer, are analyzed by assessing a) their robustness in relation to the model and b) their relation to soil moisture. Because a numerical model is more flexible for shorter periods of data compared to an analytical model (because of underlying assumptions), it can be used to relate the parameters to (daily) varying soil moisture. Third, the numerical model for heat transfer is extended to the vegetation layer, and, again, the results are compared to analytical results. The model is created by assuming homogeneity in both separate layers and by discretizing the governing heat equation over the domain. The results show that the model reproduces temperature and soil heat flux in the soil layer with similar accuracy as the analytical, harmonic model. One thermal parameter, the diffusivity, is robust and does not show a clear dependency on soil moisture. The model is however sensitive to deviations in the other parameter, the heat conductivity. The model shows a clear relation between conductivity and soil moisture, and from this, a site-specific quantitative relation is determined. This relation however is only valid in the investigated region of moisture variation and we recommend future research to cover data in a broader range of soil moisture. Overall, we conclude that the model successfully reproduced the temperature and soil heat flux throughout the full vegetation-soil continuum.

Rik Aulbers
Delft, June 2021

Contents

1

Introduction

This master thesis presents a study on heat transfer through the vegetation-soil continuum. Hereto observational analysis is combined with numerical modeling of the heat transfer processes in this complex system. Although this academic study clearly focuses on the physical principles itself, the motivation for the research originates from problems with so-called fruit-frost damage in the agricultural sector. Below we will first elaborate on the societal background for this research. The complex structure of the vegetation-soil continuum can be seen in figure 1.1.

Figure 1.1: An example of the vegetation-soil continuum. In this figure, the vegetation is grass. In this research, we assume that both layers are homogeneous. The figure shows that in reality, this is not the case: Both layers consist of organic material (dead and alive), minerals, air, and (not visible) water. Figure retrieved from [1].

Our daily weather may have large impact on agriculture. The motivation of this thesis is to combat the frost damage to fruit trees in the Netherlands during the growing period (the spring). In this period, the buds of fruit trees break, and blossoms start to grow, which will eventually develop into fruits. However, it is not uncommon that Dutch temperatures drop below 0°C in spring nights. Blossoms are sensitive to subzero temperatures and can be damaged when it freezes. Consequently, the blossoms will develop into smaller or

damaged fruits or not into fruits at all, and the (economical) yield of the orchard will be reduced. A review of the impact of spring frosts and the freezing process at the cellular level is presented in [2].

To reduce the impact of frost damage on their crops, farmers can turn to several methods. For example: Irrigation (think of overhead irrigation, man-made fog or flooding), wind machines, heaters (see figure 1.2), heat covers, or change of surface cover between trees by e.g. removing grass. Furthermore, meteorology is needed to predict the behavior of wind, temperature, precipitations (rain or snow), heat transfer, etc., as to assess which and when methods are needed. An overview of these techniques and the involved meteorology is included in [3].

Figure 1.2: An example of a method against fruit-frost. French farmers protect their vineyards with heaters against the cold. Figure retrieved from [4].

In this research, we aim at a better understanding and modeling of heat transfer, specifically heat transfer into or out of the soil, where grass-covered or bare soil and soil moisture play important roles. The temperature above grass-covered soil is cooler than above bare soil because grass acts as an insulator. This would suggest that grass removal could be beneficial for farmers: Solar heat of the daytime could be stored (and released) more efficiently over bare soil than over grass. But before those engineering methods can be applied in practice, it is important to have a solid understanding of heat transfer through bare soil and grass.

To study the heat transfer, we model the temperature and heat flux dynamics throughout the vegetation-soil continuum. First, the model is applied to only a soil layer, after which the model is extended to include both the soil and grass layers. We use a numerical method, which starts by selecting a vertical one-dimensional domain which we assume to be isotropic. In this domain, we use Fourier's law of heat conduction, which reduces to the heat equation, to calculate the temperature profile. We discretize the (continuous) heat equation (PDE) into a set of coupled equations for finite-size layers (ODE). The system of equations is then solved over time and a solution is found for the profiles of temperature and heat flux. The model will then be used to study the influence of grass and of soil moisture on the heat balance of the medium by evaluating three thermal parameters, which are called diffusivity, conductivity, and volumetric heat capacity. Diffusivity is defined as the ratio of conductivity and volumetric heat capacity. These parameters can be described as follows:

- Diffusivity: the rate of transfer of heat in material from the hot end to the cold end, in $[\mathrm{Jkg}^{-1}\mathrm{K}^{-1}]$.
- Conductivity: the ability of a material to conduct heat, in $[\mathrm{Wm}^{-1}\mathrm{K}^{-1}]$.

- Volumetric heat capacity: the amount of energy that must be added to one unit of volume of the material to cause an increase of one unit in its temperature, in $[\mathrm{Jm^{-3}K^{-1}}]$.

In a previous project in our research group ([5]), the harmonic model as described in the book of Moene and van Dam [6] was used to model the temperature and heat flux analytically. An advantage of the numerical model approach used in our project compared to the analytical, harmonic model is that the latter needs temperature observations of longer periods as input. These observations are decomposed into a Fourier series of different frequencies with different weighting factors. If the period of the input temperature is too short, the important yearly cycle may be assigned a too low weighting factor. Therefore, the harmonic model is impractical to analyze shorter periods of time. The numerical model used in this research is suitable for shorter periods of time and is, therefore, able to provide values of the mentioned thermal parameters on daily basis. The thermal parameters are then related to a provided soil moisture data set. As it is commonly known that a wet surface conducts heat better than a dry surface (think for example of cooling beverages in a dry environment or an ice bath), we expect that there will be a clear relation between the heat conductivity and the soil moisture.

The goals of the research can be summarized into three main research questions:

- Can we reproduce the temperature and soil heat flux profiles throughout a soil layer with a numerical model and are the solutions accurate in comparison with a harmonic benchmark model?
- Can we use the numerical model to estimate the thermal parameters of the soil?
  - How robust are these parameters?
  - How do these parameters relate to soil moisture?
- Can we reproduce the temperature and soil heat flux profiles throughout a two-layer system of vegetation and soil?

To answer these questions and thereby assess the numerical model, two data sets are used. The first is a data set from the meteorological site at Haarweg, The Netherlands, provided by Wageningen University & Research. The second set is from the lysimeter field at the USDA-ARS Conservation & Production Research Laboratory in Bushland, Texas, The United States of America. Both data sets provide measurements of soil temperature, soil heat flux, and soil moisture. Furthermore, the Haarweg data set provides measurements of longwave outgoing radiation, from which grass temperature can be calculated.

Chapter 2 explains the theory of heat diffusion and the relevance of the thermal parameters. Then, in chapter 3, the data sets are illustrated and the numerical method and parameter optimization are explained. Thirdly, chapter 4 provides and analyzes the results, after which chapter 5 concludes the research. Appendix A and B provide additional results of the research. The project is carried out in the Atmospheric science group at the Department of Geoscience and Remote Sensing, Faculty of Civil Engineering, at Delft University of Technology. The supervisors are prof. dr. ir. Bas van de Wiel, dr. ir. Marie-Claire ten Veldhuis, dr. ir. Steven van der Linden and ir. Judith Boekee.

2

Theory

2.1. Heat transfer in a homogeneous medium

In this research, we will assume that soil is a homogeneous medium. This is not truly the case, because soil exists of organic material (flora and fauna), moisture, clay, air cavities, et cetera, which can be seen in figure 1.1 and is schematically depicted in figure 2.1. Where on microscale the soil is a composite, we here assume it to be a (homogeneous) continuum since we are only interested in the overall behavior of the soil temperature. Furthermore, it would be too complicated to model all individual components. If we assume that the soil has

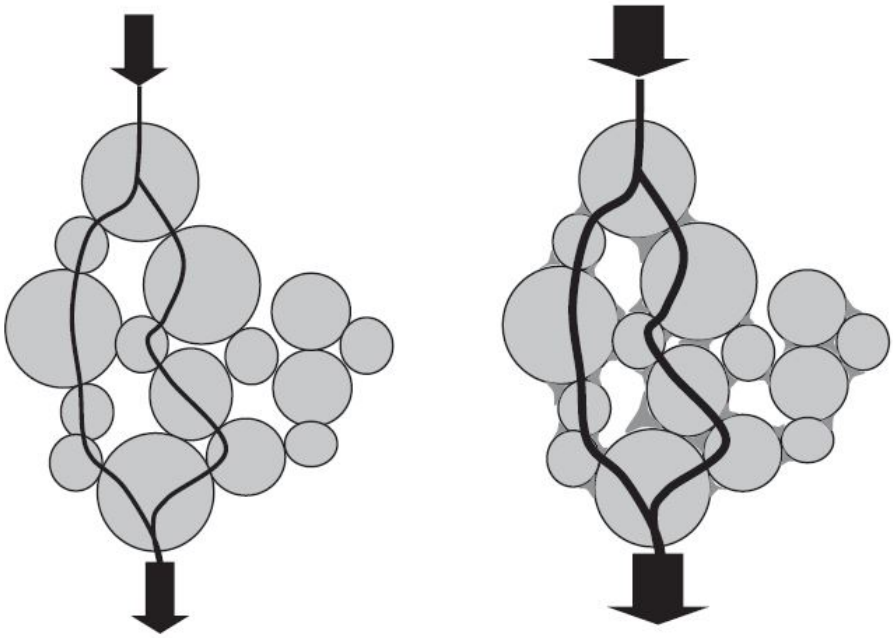

Figure 2.1: Schematic representation of conduction of heat through the soil. The circles denote the soil particles. The space between particles is filled with air (white) and moisture (dark grey). The arrows denote the conduction of heat. Figure retrieved from p.49 [6].

no velocity, there is no source/sink of heat in the soil, that the problem is only one-dimensional because of the homogeneity in the x and y-direction, and that the parameters λ, ρ, c and κ are constant over space and time, Fourier's law reduces to

$$\frac{\partial T}{\partial t} = \frac{\lambda}{\rho c}\frac{\partial^2 T}{\partial z^2} = \kappa \frac{\partial^2 T}{\partial z^2}. \tag{2.1}$$

In this equation, T denotes the temperature in [K] or [°C], t the time in [s], λ the thermal conductivity in [$\mathrm{Wm^{-1}K^{-1}}$], c the specific heat capacity in [$\mathrm{Jkg^{-1}K^{-1}}$], ρ the density in [$\mathrm{kgm^{-3}}$], κ the thermal diffusivity

in [m^2s^{-1}] and z the depth in [m]. For convenience, $\hat{z}$ is defined positive downward into the ground with $z = 0$m located at the top of the soil layer. The product of $\rho c = C$ is sometimes referred to as volumetric heat capacity in [$Jm^{-3}K^{-1}$]. If we want to solve equation 2.1 for $T(z,t)$ with a numerical scheme, we have to set two boundary conditions (BC's) and one initial condition (IC), which will be explained in chapter 3.

According to [6], heat transport in the soil is dominated by thermal conduction, which means the soil heat flux density G (in [Wm^{-2}]) is defined by the local temperature gradient and the thermal conductivity:

$$G = -\lambda \frac{\partial T}{\partial z}. \tag{2.2}$$

If we have an expression for $T(z,t)$ and for λ, we can solve equation 2.2 for the soil heat flux $G(z,t)$.

2.1.1. Heat transfer in a two-layer system of separate homogeneous media

Here, we seek to model the vegetation-soil (or grass-soil) continuum by connecting two homogeneous media. These two media, vegetation and soil, have similar diffusion equations, but with different effective parameters. In those media we describe thermal heat diffusion according to the following equations:

$$\frac{\partial T_{veg}}{\partial t} = \frac{\lambda_{veg}}{\rho_{veg} c_{veg}} \frac{\partial^2 T_{veg}}{\partial z^2} = \kappa_{veg} \frac{\partial^2 T_{veg}}{\partial z^2}, \tag{2.3a}$$

$$\frac{\partial T_{soil}}{\partial t} = \frac{\lambda_{soil}}{\rho_{soil} c_{soil}} \frac{\partial^2 T_{soil}}{\partial z^2} = \kappa_{soil} \frac{\partial^2 T_{soil}}{\partial z^2}, \tag{2.3b}$$

where the subscripts 'veg' and 'soil' stand for the 'vegetation'-medium and the 'soil'-medium respectively. The two media are attached and need to have two additional boundary conditions at $z = 0$m: Both T and its vertical derivative should be continuous. The vegetation of the Haarweg data set is a grass layer and is assumed to be a homogeneous medium with a thickness of (approximately) 10cm. It spreads in the coordinate system from $z = -0.1$m to $z = 0$. Note again that $\hat{z}$ is defined positive when directed into the soil. Again we note that in reality grass is far from homogeneous (see figure 1.1), but it is interesting to see how close we can get to solving the problem with such a simplification.

2.2. Thermal parameters of soil

Figure 2.1 shows that the soil exists of three main components: soil particles, air, and water (please bare in mind that soil particles are also a group of other particles, for example, quartz, clay minerals, and organic material). For some of the parameters, i.e. density and heat capacity, the overall parameter of the soil is the combination of the weighed parameters of the three components, which can be represented as

$$\rho_s = f_p \rho_p + \theta \rho_w + f_a \rho_a \tag{2.4a}$$

$$C_s = f_p C_p + \theta C_w + f_a C_a \tag{2.4b}$$

$$c_s = C_s / \rho_s. \tag{2.4c}$$

In this equation, the subscript 'p' denotes (soil) particles, 'w' denotes water, and 'a' air, and f_p, θ and f_a are the associated volumetric fractions in [m^3m^{-3}], or [-]. Equation 2.4 shows that both the density and the volumetric heat capacity depend linearly on the soil moisture content.

The situation of the other free parameter (the conductivity λ) is, however, more complex. Whereas soil particles have rather large conductivity, the air has a conductivity close to an insulator. When soil is completely dried out, the conductivity is effectively determined by the total surface area between soil particles. Adding a small amount of water would therefore have a substantial effect. Figure 2.1 shows that the water tends to concentrate around the areas of contact so that the conduction area increases and the overall conductivity increases too. Adding more water would increase the conductivity even more, but not as dramatically as in the (almost) dry regions because the conductivity of water is much lower than that of the soil material.

The third parameter, the diffusivity κ, is defined as the ratio of conductivity and volumetric heat capacity, $\frac{\lambda}{C}$, as can be seen in equation 2.1. In the dry region, this ratio increases with moisture, because the numerator (λ) increases more than the denominator (C). So, in the dry region, the diffusivity increases with moisture. In the wetter region, the increase in λ slows down, while the increase in C remains linear. After a certain point, the ratio $\frac{\lambda}{C}$ decreases with moisture and so does the diffusivity. The relations are depicted by [6] and can be found in figure 2.2. Note that figure 2.2 does not show any quantitative results on the x- or y-axis and is hence

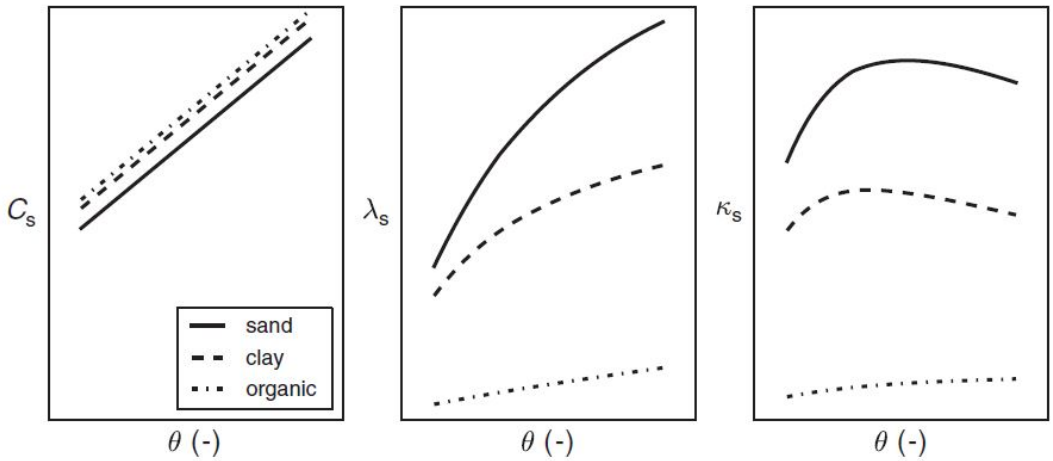

Figure 2.2: Schematic representation of the relation of volumetric heat capacity C, conductivity λ, and diffusivity κ with soil moisture θ for sand, clay, and organic material. The subscript 's' of the parameters denotes the soil. Figure retrieved from p.51 [6].

just meant as a schematic. A goal in this study is to actually quantify those dependencies on soil moisture.

3

Method

3.1. Data sets

3.1.1. Haarweg, The Netherlands

The first data set used in this research was obtained at the Haarweg measurement site located in the center of The Netherlands (lat. 51°58'N, long. 5°38'W, altitude 7msl; `www.met.wau.nl`) and is described in detail in [7], [8] and [9]. The soil consists predominantly of "heavy basin clay resulting from the back-swamps of the Rhine river" [7]. We used the data from 16-May-2001 up until 14-Nov-2012, for which data with a high temporal resolution is available (i.e. 10-minute coverage).

A schematic overview of the measurements is presented in figure 3.1. The figure shows three domains: Atmosphere (blue), the vegetation layer (green), and the soil (orange) (covered by vegetation or bare surface). Please note again that $\hat{z}$ is defined positive downward into the ground with $z = 0$m located at the top of the soil layer. In the figure, T denotes measured temperature (soil or radiation), G denotes measured soil heat flux and Θ denotes measured soil moisture. The subscripts '5cm', '10cm', and '20cm' stand for depth in the soil, the subscript 'IRT' stands for radiation (temperature), and the superscripts 'bare' and 'grass' stand for bare soil or grass-covered soil.

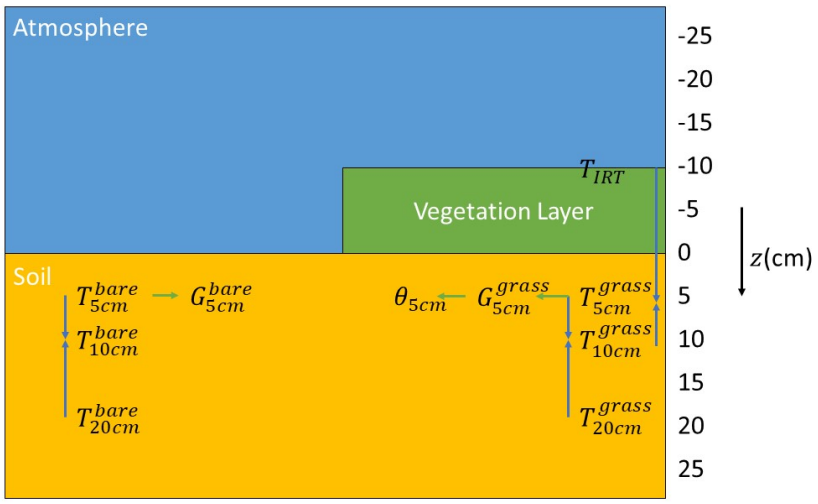

Figure 3.1: Schematic representation of the used measurements and models. The system consists of three domains: Atmosphere (blue), the vegetation layer (green), and the soil (orange) (covered by vegetation or bare soil). Each combination of two blue arrows denotes a domain. The green arrows denote the calculation of soil heat flux out of temperature or the relation of the parameters to soil moisture.

In the bottom left part, figure 3.1 shows the measurements used in the one-layer model for bare soil. T_{5cm}^{bare} and T_{20cm}^{bare} form the boundaries of the domain in which $T(z,t)$ is calculated. Then, the parameter for diffusivity is optimized by comparing the modeled and the measured temperature T_{10cm}^{bare} at 10cm, which is denoted by the blue arrows. The optimization process will be explained in section 3.3. The soil heat flux is calculated from the modeled profile of $T(z,t)$ and compared to the measured heat flux G_{5cm}^{bare} at 5cm to optimize the conductivity, which is denoted by the green arrow.

Similarly, the one-layer model for grass-covered soil is depicted in the bottom right part of the figure. T_{5cm}^{grass} and T_{20cm}^{grass} form the boundaries of the domain in which $T(z,t)$ is calculated. The modeled temperature is again compared to the measured temperature T_{10cm}^{grass} at 10cm to optimize the diffusivity. Then, the soil heat flux is calculated from the profile of $T(z,t)$ and compared to the measured heat flux G_{5cm}^{grass} to optimize the conductivity. Lastly, the optimized parameters for diffusivity and conductivity can be related to the measured soil moisture at 5cm depth, which is denoted by Θ_{5cm}. Note in this part of the figure that the soil moisture is only measured beneath grass-covered soil. Because we assume homogeneity, the diffusivity, optimized at 10cm depth, can still be related to the soil moisture, measured at 5cm depth.

Lastly, at the total right side of figure 3.1, the two blue arrows denote the two-layer model. The boundaries of the domain are now the radiation temperature of the grass T_{IRT} at -10cm and the soil temperature T_{10cm}^{grass} at 10cm depth. The two values of the diffusivity (both for the grass layer and for the soil layer) are now optimized by comparing the modeled temperature profile $T(z,t)$ to the measured temperature T_{5cm}^{grass} at 5cm depth. Again, the soil heat flux is calculated from the temperature profile and compared to the measured soil heat flux profile G_{5cm}^{grass} to optimize the soil conductivity parameter. The parameters in the two-layer model are not related to the soil moisture as it would not provide any additional information.

The sensors of the Haarweg data used in this research can be found in table 3.1.

Table 3.1: In this research, the soil temperatures T at 5cm, 10cm, and 20cm depth and the soil heat flux G at 5cm are used for both grass-covered soil and bare ground. The longwave radiation L_{out} is measured above grass soil and is used to calculate the radiation temperature T_{IRT} of the grass top. Note that a negative value for z translates to above soil.

Name	Unit	z [m]	Sensor	Grass-covered soil	Bare soil
T_{5cm}	°C	0.05	Pt100	✓	✓
T_{10cm}	°C	0.10	Pt100	✓	✓
T_{20cm}	°C	0.20	Pt100	✓	✓
G_{5cm}	Wm^{-2}	0.05	TNO-WS31	✓	✓
L_{out}	Wm^{-2}	-0.10	Kipp CG2	✓	x

The longwave radiation mentioned in table 3.1 is used to calculate the radiation temperature via

$$T_{IRT} = (\frac{L_{out}}{\epsilon\sigma})^{\frac{1}{4}}, \tag{3.1}$$

in which $\epsilon = 0.99$, the assumed emissivity of grass [10], and $\sigma = 5.67 \cdot 10^{-8} Wm^{-2}K^{-4}$, the Stefan-Boltzmann constant. The soil heat flux G_{5cm} is measured with a heat flux plate (TNO-WS31) and must be corrected for instrumental shape and for the difference between plate and soil conductivities [7] with the factor Φ:

$$\Phi = \frac{1}{1 - 1.7tA^{-0.5}(1 - \epsilon_p^{-1})}. \tag{3.2}$$

In equation 3.2, t = 2mm, the thickness of the plate, $A = \frac{1}{4}\pi 0.11^2 m^2$, the area of the plate, and $\epsilon_p = \frac{\lambda_{plate}}{\lambda_{soil}}$, the ratio between the thermal conductivity of the plate to that of the soil. Note that the correction factor is a function of λ_{soil}, which will become important in the optimization process. The measurement locations are photographed and depicted in figure 3.2.

To model the relations as described in section 2.2, an additional data set with soil moisture is used, which is not included in table 3.1 (but is included in figure 3.1). The soil moisture is measured by a Time-Domain Reflectometry System (TDR100 Reflectomer, [11]) with an interval time of 60 minutes. The logger is located at lat. 51°97'N, long. 5°64'W and the sensors are located in a triangle at 8.5m north, 8.5m west, and 8m north around the logger as to measure an 'area average value'. The sensors are located beneath grass-covered surfaces and are located at different depths: 0cm, 2.5cm, 5cm, 10cm, 30cm, and 60cm. We are interested in

(a)

(b)

Figure 3.2: Figure (a) shows the longwave radiation sensor (Kipp CG2). Figure (b) shows the temperature and soil heat flux measurement locations for bare soil and grass soil. The sensors for temperature (Pt100) and soil heat flux (TNO-WS31) are buried beneath the surface. Note also that the grass is mowed to an average height of 10cm. Figures retrieved from p.21 and p.23 [9].

the relation of soil moisture with the parameter λ defined at 5cm depth as can be seen in figure 3.1. Therefore we only use the 5cm moisture measurements and we average over the three positions via equation 3.3:

$$\theta_{5cm} = \frac{1}{3}(\theta_{5cm}^{8.5mNorth} + \theta_{5cm}^{8.5mWest} + \theta_{5cm}^{8.0mNorth}). \tag{3.3}$$

3.1.2. Texas, U.S.A.

During the project, a second data set is used to validate the model a second time. The data set is described in detail in [12] and in [13] and contains soil temperature, soil heat flux, and soil moisture data. The measurements were made from 24 June to 24 September 2008 at the USDA-ARS Conservation & Production Research Laboratory (Bushland, Texas, USA). We used the data as specified in table 3.2. The measurements for Θ_{6cm}

Table 3.2: In this research, the temperature T at 4cm, 8cm, and 16cm depth and the soil heat flux G at 8cm are used. The soil moisture Θ at 6cm and at 12cm depth is used to calculate Θ at 8cm.

Name	Unit	z [m]	Sensor
T_{4cm}	°C	0.04	TDR probe - copper-constantan thermocouple
T_{8cm}	°C	0.08	TDR probe - copper-constantan thermocouple
T_{16cm}	°C	0.16	TDR probe - copper-constantan thermocouple
G_{8cm}	Wm^{-2}	0.08	HFT-3.1
Θ_{6cm}	[-]	0.06	Trifilar TDR probes
Θ_{12cm}	[-]	0.12	Trifilar TDR probes

and Θ_{12cm} are used to calculate Θ_{8cm} as a weighted average. All the measurements were done at 10 different locations close to each other. In this research, we take the average of the 10 locations to do the parameter optimization. The procedure and results of this second data set are described in appendix B.

3.2. Discretizing the unsteady one-dimensional heat diffusion equation

We aim to solve equation 2.1 in a numerical way, for which we will use a method described in chapter 6 of [14]. The method is often referred to as the 'FTCS' (Forward Time Centered Space) method. As explained in section 2.1, we assume that the parameters λ, c, ρ, and κ are constant over space and time (for the selected domain and period). Furthermore, we substitute x for z. We integrate equation 2.1 over the time interval from t to $t+\Delta t$ and over a 1D control volume from west to east (which is pure terminology and can be replaced for instance by top and bottom) and we get

$$\rho c \Delta x (T_p^{j+1} - T_p^j) = \int_t^{t+\Delta t} [\frac{\lambda(T_E - T_P)}{\delta x_e} - \frac{\lambda(T_P - T_W)}{\delta x_w}] dt. \tag{3.4}$$

In this equation, the uppercase subscripts 'E','P' and 'W' denote a location at the side of a control volume, and the smaller case subscripts 'e' and 'w' denote a location in the middle of a control volume ('e' between 'E' and 'P', 'w' between 'P' and 'W') as can be seen in figure 3.3. 'j' denotes the discretization of time. In this

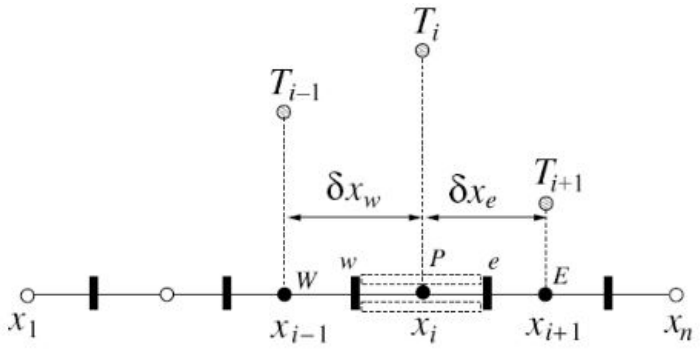

Figure 3.3: The figure shows how 1D discretization schematically looks like. 'W' denotes west and 'E' denotes east. Figure retrieved from p.121 [14].

derivation, we have assumed linear interpolation for the characteristic cell faces:

$$\int_w^e \frac{\partial^2 T}{\partial x^2} dx = (\frac{dT}{dx})_e - (\frac{dT}{dx})_w = \frac{T_E - T_P}{\delta x_e} - \frac{T_P - T_W}{\delta x_w}. \tag{3.5}$$

We then assume that time integration of T results in a combination of 'old' time T^j and 'new' time T^{j+1}

$$\int_t^{t+\Delta t} T_P dt = [f T_P^{j+1} + (1-f) T_P^j)] \Delta T, \tag{3.6}$$

where f is a weighting factor and 'P' may be replaced by 'E' or 'W'. For an explicit scheme, as we will use, $f = 0$. We combine equations 3.4 and 3.6 and end up with:

$$\frac{\rho c \Delta x T_P^{j+1} - T_P^j}{\Delta t} = [\frac{\lambda(T_E^j - T_P^j)}{\delta x_e} - \frac{\lambda(T_P^j - T_W^j)}{\delta x_w}]. \tag{3.7}$$

On a uniform grid, as we will use, $\delta x_e = \delta x_w$. We generalize the iteration of equation 3.7 over space by replacing 'E' with 'i+1', 'P' with 'i' and 'W' with 'i-1', in which 'i' denotes the discretization of space. By rearranging, substituting z back for x again and substituting $\kappa = \frac{\lambda}{\rho c}$, the result is

$$T_i^{j+1} = T_i^j + \frac{\kappa \Delta t}{\Delta z^2}(T_{i+1}^j - 2T_i^j + T_{i-1}^j). \tag{3.8}$$

If we now discretize the control volume, define one initial condition (IC) and two boundary conditions (BC's), we can calculate $T(z,t)$ over the discretized space ('i') and time ('j') domain. This process will be described in detail in section 3.3.

3.2.1. Neumann stability analysis

If we regroup equation 3.8, we get

$$T_i^{j+1} = (1 - 2\frac{\kappa \Delta t}{\Delta z^2})T_i^j + \frac{\kappa \Delta t}{\Delta z^2}(T_{i+1}^j + T_{i-1}^j). \tag{3.9}$$

One of the four principles of the discretization procedure is that the coefficient connected to T_i^j should be positive at all times (p. 124 [14]). This means that

$$1 - 2\frac{\kappa \Delta t}{\Delta z^2} > 0, \tag{3.10}$$

or

$$\frac{\kappa \Delta t}{\Delta z^2} < \frac{1}{2}. \tag{3.11}$$

As will follow from section 3.3, we construct the model with values for Δt and for κ, which means that we end up with the following condition for Δz:

$$\Delta z > \sqrt{(2\kappa \Delta t)}. \tag{3.12}$$

Condition 3.12 is derived using von Neumann stability analysis and ensures a numerically stable FTCS scheme. The numerical convergence (and stability) are demonstrated in practice by comparing numerical results to known analytical solutions.

3.2.2. Two-layer model

For the two-layer model (vegetation-soil) we follow a similar approach, only now the parameters are not constant over space. Similarly as for 3.8, we end up with equation 3.13:

$$T_P^{j+1} = T_P^j + \frac{\Delta t}{\Delta z^2}(\kappa_e(T_E^j - T_P^j) - \kappa_w(T_P^j - T_W^j)), \tag{3.13}$$

or

$$T_i^{j+1} = T_i^j + \frac{\Delta t}{\Delta z^2}(\kappa_{i+0.5}(T_{i+1}^j - T_i^j) - \kappa_{i-0.5}(T_i^j - T_{i-1}^j)). \tag{3.14}$$

κ can have two values: If $z > 0$, $\kappa = \kappa_{soil}$, and if $z < 0$, $\kappa = \kappa_{veg}$.

3.2.3. Discretizing the soil heat flux equation

Equation 2.2 is rather easy to discretize. As will be explained in 3.3, we will have to use a forward difference scheme and we calculate the soil heat flux at $z = 0.05$m via

$$G(0.05\text{m}, t) = -\lambda \frac{T(0.05\text{m} + \Delta z, t) - T(0.05\text{m}, t))}{\Delta z}. \tag{3.15}$$

3.3. Parameter optimization procedure

This section describes step-by-step how the optimal parameters for the diffusivity κ and conductivity λ are determined.

1. First, a grid of expected values for κ and λ is created. This is the so-called 'shooting method'. $\Delta t = 30$s is chosen, which is relatively small compared to the measurement time interval of 600s. The domain is created from $z = 0.05$m up until 0.20m. The minimum value of Δz follows from condition 3.12 where the largest possible value of κ is taken as an upper limit. For convenience, Δz is rounded off (conservatively) to its closest value of 1, 2.5, 5, or 10 mm. The control volume is discretized with step size Δz. For example, if the maximum value of κ is set to $\kappa_{max} = 10 \cdot 10^{-7}\text{m}^2\text{s}^{-1}$, $\Delta z > \sqrt{(2\kappa_{max}\Delta t)} = 7.8$mm and is rounded up to $\Delta z = 10$mm. Furthermore, the measured data is cut to a certain period. In this research, these periods are either a single day or a sequence of days in the period 01/05/2006 - 31/10/2006. The months May-October are chosen to omit temperatures below 0°C as to avoid phase transitions of water. Frozen water (either snow or ice) has important repercussions on the surface energy balance (section 2.3.8 of [6]). The year 2006 is chosen because it shows a relatively large range of soil moisture compared to the other possible years, which is beneficial to investigate the relations of figure 2.2.

2. For the initial condition (IC) $T(z,0)$, we use spline interpolation over the measured temperatures T_{5cm}, T_{10cm} and T_{20cm} to the domain with space step Δz. The boundary conditions (BC's) used are the measured temperatures T_{5cm} and T_{20cm}, which are interpolated from the measurement interval 600s to the new interval 30s.

3. Third, we use equation 3.8 to calculate the new temperature $T(z,30\text{s})$. This process is repeated each time with interval 30s until $T(z,t)$ is calculated for the total desired period. To save memory, only the temperatures at intervals of 600s are stored.

4. The root-mean-square error e_T is calculated for the modeled temperature as a function of the preset κ:

$$e_T(\kappa) = \sqrt{\frac{1}{N}\sum_{j=1}^{N}(T_j^{\text{obs}} - T_j^{\text{mod}}(\kappa))^2} \tag{3.16}$$

   In this equation, j denotes a point in the time-series, with maximum N. Note that $t_j = (j-1)\Delta t$ and that $\Delta t = \frac{P}{N-1}$, where P is the period. e_T is a function of the inserted κ. By calculating e_T for all possible values of κ, the minimum error, and corresponding κ, κ_{opt}, can be found. This must be a global minimum, or the range of κ at step 1 will be broadened. For a visualisation of this process, see figure 4.2. T^{obs} is the measured temperature, T_{10cm}, and T^{mod} is the modeled temperature at 0.10m, $T(0.10\text{m}, t)$.

5. With the optimized profile $T(z,t)$, a similar optimization can be executed to find the optimal λ. The measured G_{5cm} has to be corrected with the factor Φ (equation 3.2). Because G is measured at 0.05m and the domain goes from $z = 0.05$m up until 0.20m, the forward difference method of equation 3.15 is necessary. The optimal value for λ, λ_{opt}, is then found by minimizing the error of the soil heat flux, e_G:

$$e_G(\lambda) = \sqrt{\frac{1}{N}\sum_{j=1}^{N}(G_j^{\text{cor}}(\lambda) - G_j^{\text{mod}}(\lambda))^2}, \tag{3.17}$$

   where G^{cor} is the measured soil heat flux at 0.05m corrected with the factor Φ (equation 3.2, $G^{cor} = G^{obs}\Phi^{-1}$) and G^{mod} is the modeled heat flux at 0.05m.

The procedure results in optimal values for κ and λ for the chosen period. In this research, we will first analyze the quality of the model by optimizing over a period of multiple days. Then we will optimize the parameters over individual days and relate the results to the (daily) mean soil moisture variations.

3.3.1. Two-layer model

The procedure for the two-layer model is very similar. In the following enumeration, the differences are shortly highlighted.

1. The domain now is from $z = -0.10$m up until 0.10m. Furthermore, the diffusivity is a (step)function of z, i.e. $\kappa = \kappa(z)$ (if $z < 0$m, $\kappa = \kappa_{veg}$, if $z > 0$, $\kappa = \kappa_{soil}$). A range is created for possible values of κ_{veg} and κ_{soil}.

2. Whereas the mean temperatures for 2006 were nearly uniform in depth in the upper soil, for the vegetation an off-set of 0.9°C in the yearly mean was found: $\overline{T_{5cm}^{2006}} = \overline{T_{10cm}^{2006}} = \overline{T_{20cm}^{2006}} = 12.0\,^{\circ}\text{C}$ and $\overline{T_{IRT}^{2006}} = 11.1\,^{\circ}\text{C}$. As described in the book [6], the yearly means should be equal if we assume that there are no heat sources or sinks (on this time scale). Therefore, for all the measurements the yearly mean is subtracted such that the used signals are averaged around 0°C. For the initial condition, we use spline interpolation over the radiation temperature T_{IRT} (equation 3.1) and over the measured temperatures T_{5cm} and T_{10cm} to the domain with step size Δz. The boundary conditions are T_{IRT} and T_{10cm}, which are again interpolated. Furthermore, T and its derivative must be continuous at the interface $z = 0$m. In a discretized domain however these requirements are only approximated, because the temperature is only defined at the sides or in the middle of the discretized control volumes. Therefore, the discretization should be fine enough near the interface as to accurately estimate and to prevent 'unnatural kinks' in the vertical temperature profile.

3. We use equation 3.14 to calculate the new temperature profile over the entire period.

4. To find the optimal parameters, equation 3.16 is used. The difference is that the modeled temperature now is a function of both soil and vegetation diffusivities: $T_j^{mod} = T_j^{mod}(\kappa_{soil}, \kappa_{veg})$. Furthermore, the measured and modeled temperature of equation 3.16 are now compared at $z = 0.05$m, whereas the temperatures of the one-layer model were compared at 0.10m.

5. The calculation of G_{5cm} in the two-layer method is not done with a forward difference scheme but with a central difference scheme because the domain is not limited at $z = 0.05$m. The central difference scheme reads
$$G(0.05\text{m}, t) = -\lambda \frac{T(0.05\text{m} + \Delta z, t) - T(0.05\text{m} - \Delta z, t))}{2\Delta z}. \tag{3.18}$$
The parameter λ is again optimized by minimizing the error in G calculated with equation 3.17.

4

Results and Discussion

4.1. Modeling heat transfer in soil

As stated in the first research question, we investigate whether it is possible to model the soil as a homogeneous medium and solve for the temperature $T(z,t)$ and soil heat flux $G(z,t)$ with an explicit numerical scheme. As described in section 3.3, a part of the first step is to cut the signal into the desired period. In the proceeding section, we use the period 07/07/2006-17/07/2006. Figure 4.1 shows the observed temperature underneath a bare soil surface and a grass-covered surface.

The figure shows that the amplitudes (extrema) for bare soils (4.1a) are larger than that of grass-covered soils (4.1b), which is stressed by plotting them on the same scale. This is 'the insulating effect of grass' and will be further discussed in section 4.4. Furthermore, we see that the amplitude decreases with depth and that the phase shifts to the right. The book of Moene and van Dam [6] shows that this behavior can be explained by prescribing soil temperature as (a summation of) sinuses. Here, we will briefly demonstrate the concept with a single sinus. Let's assume that we have a semi-infinite homogeneous soil where at the surface ($z = 0$m) the temperature is prescribed as

$$T(0,t) = \overline{T} + A(0)\sin(\omega t). \tag{4.1}$$

In this equation, $\overline{T}$ is the mean and $A(0)$ is the amplitude in [K] or [°C] and ω is the frequency of the wave in [s^{-1}]. The lower boundary condition is $T(\infty,t) = \overline{T}$, and the solution of the problem is

$$T(z,t) = \overline{T} + A(z)\sin(\omega t - \frac{z}{D}). \tag{4.2}$$

In this equation, the amplitude is (indeed) decreasing with depth as

$$A(z) = A(0)e^{-z/D} \tag{4.3}$$

and D is the damping depth in [m] given by

$$D \equiv \sqrt{\frac{2\kappa}{\omega}}. \tag{4.4}$$

Equation 4.2 shows that the phase of the signal indeed shifts over depth.

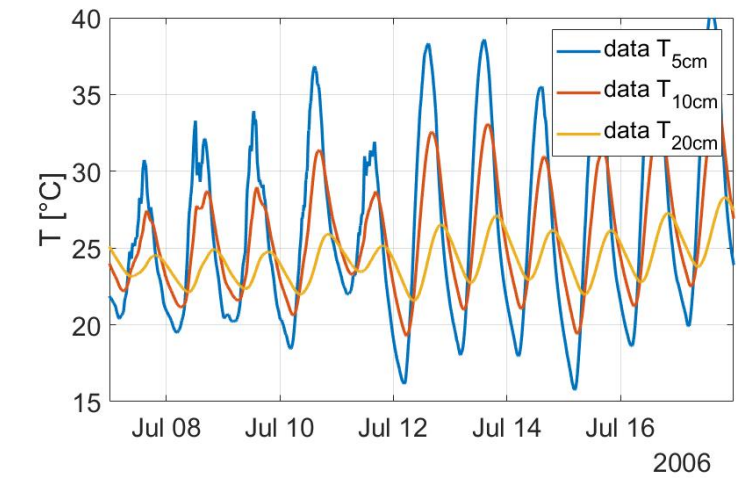

(a)

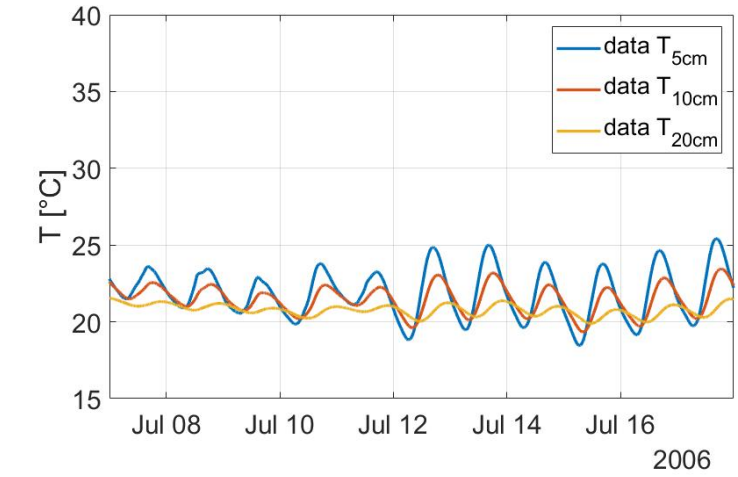

(b)

Figure 4.1: In the figure, the temperature data for depths of 5, 10 and 20cm are given for the period 07/07/2006-17/07/2006. Figure (a) represents a bare soil, figure (b) represents a grass-covered soil.

Step 2 of the procedure was to set an IC and two BC's. The IC is created by using spline interpolation over the temperatures T_{5cm}, T_{10cm}, and T_{20cm} at 07/07/2006 00:00:00 to the domain with Δz = 1cm. The BC's are the measurements of T_{5cm} and T_{20cm}, which are interpolated from the measurement interval 600s to the time step interval Δt = 30s. As mentioned in section 3.3, the modeled temperature is compared to the measured temperature at 10cm depth (which is shown in red in figure 4.1) to optimize the diffusivity. This process is visualized in figure 3.1.

The use of spline interpolation to create the initial condition will probably cause some errors. During the project, other approaches have been studied as well, for example, an initial temperature profile constant over height, a linear interpolation between the used signals, or using the FTCS scheme twice (to first create an initial condition after which the rest of the temperature is calculated). Spline interpolation was the best choice because its performance was good enough and the computational cost was not too high.

Steps 3 and 4 of the procedure are performed by calculating $T(z,t)$ for different values for κ and minimizing the difference between the model predicted and the observed temperature. Figure 4.2 shows the calculated error e_T plotted against the inserted κ_{soil}, for both the bare and grass-covered soil.

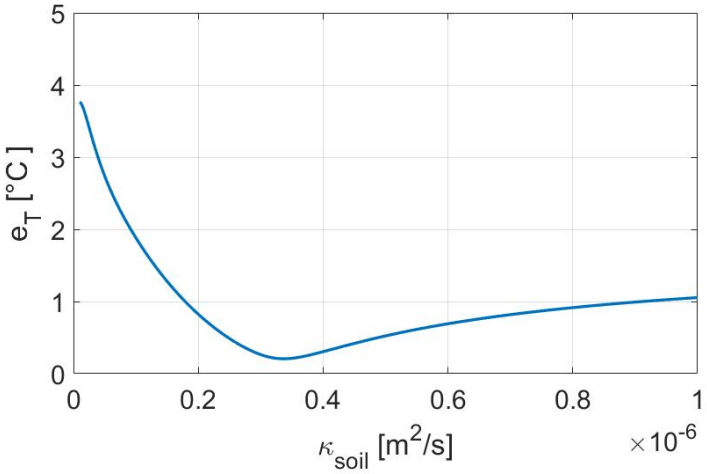

(a) Minimum is located at $\kappa_{soil} = 3.37 \cdot 10^{-7}$ m^2/s and $e_T = 0.21$ °C.

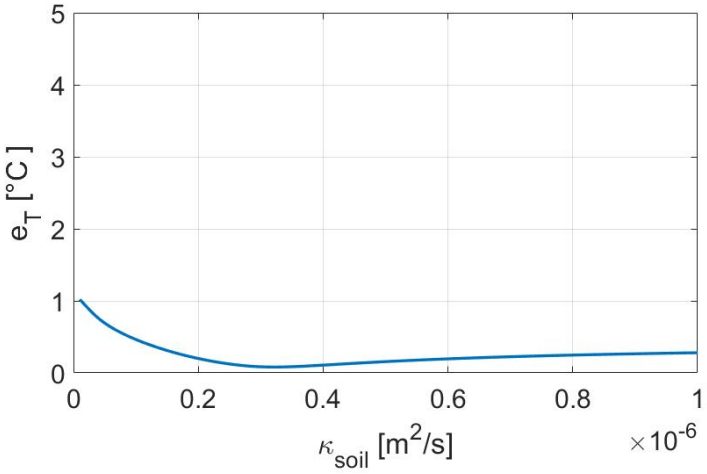

(b) Minimum is located at $\kappa_{soil} = 3.22 \cdot 10^{-7}$ m^2/s and $e_T = 0.08$ °C.

Figure 4.2: The error e_T is plotted against κ_{soil} for soil underneath bare surface (a) and for soil under grass surface (b) for the period 07/07/2006-17/07/2006.

The optimal parameters are $\kappa_{soil} = 3.37 \cdot 10^{-7}$ m^2/s for mineral soil underneath bare surface and $\kappa_{soil} = 3.22 \cdot 10^{-7}$ m^2/s for mineral soil underneath grass surface. The minimum errors are then respectively $e_T = 0.21$ °C and $e_T = 0.08$ °C. Both curves have a remarkably similar 'L'-shaped form: the lines are steep on the left side of the minimum, whereas they are smooth on the right side of the minimum. Mathematically, this translates to a large gradient left to the minimum and a small gradient right to the minimum. Practically this means that the model is more sensitive for a too low value of κ_{soil} than for a too high value. This is an important result that will come back in section 4.4. The figure also shows that the error for bare soil is overall larger than that of grass-covered soil. Equation 3.16 shows that this makes sense, as the magnitude of the error scales with the square root of the residuals. Figure 4.1 shows that bare soil has greater extrema than grass-covered soil, so any error in the model is enlarged. To generalize the error plots, one could choose to normalize the error calculation with the amplitude of the signal. In figure 4.2, the scaling factor between the two plots is about 4, which is similar to the scaling factor between the amplitudes plotted in figures 4.1a and 4.1b.

Figures 4.3a and 4.3b show the measured temperature and the modeled temperature at $z = 10$cm depth for the optimal value for κ_{soil} (that is, the lowest value for e_T). Note that the measured temperature plotted in blue is nearly invisible as both lines are almost overlying.

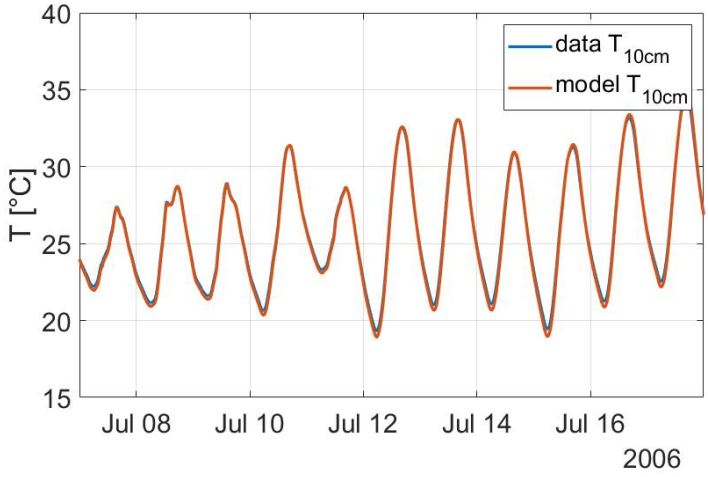

(a) $\kappa_{soil} = 3.37 \cdot 10^{-7}$ m^2/s and $e_T = 0.21$ °C.

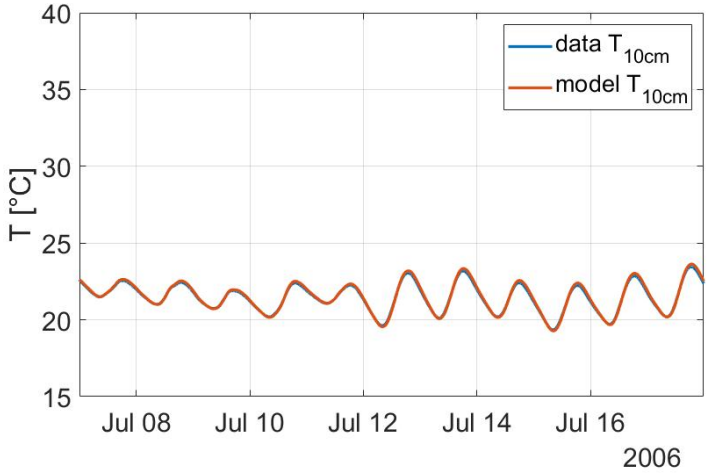

(b) $\kappa_{soil} = 3.22 \cdot 10^{-7}$ m^2/s and $e_T = 0.08$ °C.

Figure 4.3: The measured and modeled temperature at 10 cm depth for bare soil (a) and grass-covered soil (b). Note that the blue line is nearly invisible as both lines are almost overlying.

The numerical model seems to work very well as both lines almost coincide. This answers (a part of) the first research question and shows that indeed it is feasible to model soil temperature dynamics with a (relatively) simple numerical scheme assuming homogeneous soil properties. Hereby the scheme uses two given boundary conditions and one initial condition. One could argue that the chosen domain (0.05m up to 0.20m) and the chosen period (07/07/2006-17/07/2006) are respectively small and short. During the project, larger domains and longer periods have been studied with similar results (not shown). The domain can be stretched up to a depth of 1m (limited by the data set) and the period can be extended up to months or even years. This report however is a proof of principle. Extension to larger domains and longer time intervals is beyond our scope here.

To answer the first research question, a comparison is made with the results of the harmonic model[1], which are given in figure 4.4:

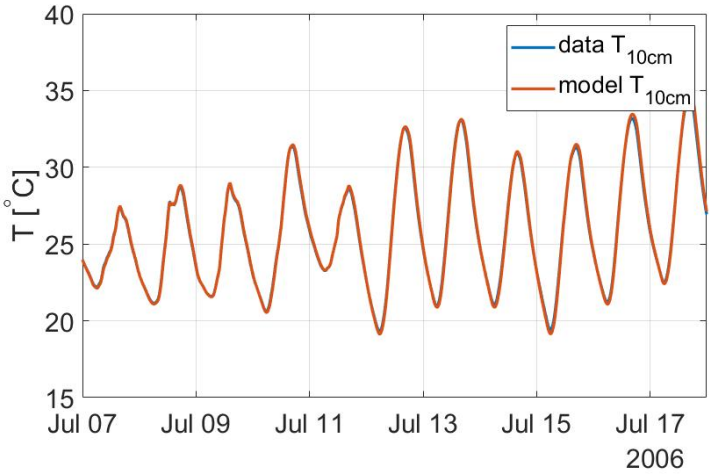

(a) $\kappa_{soil} = 3.28 \cdot 10^{-7}$ m^2/s and $e_T = 0.20$ °C.

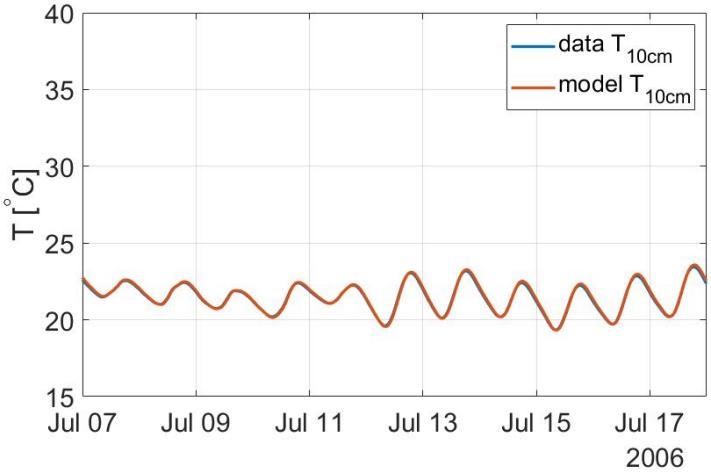

(b) $\kappa_{soil} = 3.03 \cdot 10^{-7}$ m^2/s and $e_T = 0.10$ °C.

Figure 4.4: The measured and modeled temperature at 10 cm depth for bare soil (a) and grass-covered soil (b) for the **harmonic** model. The results are very similar to that of the numerical model depicted in figure 4.3.

The figure shows that the results are extremely similar and that the errors are of the same order of magnitude: The error for soil under bare surface now is $e_T = 0.20$ °C instead of $e_T = 0.21$ °C, and soil under grass surface now is $e_T = 0.10$ °C instead of $e_T = 0.08$ °C. The optimal diffusivities of the harmonic model are somewhat lower than that of the numerical model: For bare surface, $\kappa_{soil} = 3.28 \cdot 10^{-7}$ m^2/s instead of $\kappa_{soil} = 3.37 \cdot 10^{-7}$ m^2/s, and for grass surface, $\kappa_{soil} = 3.03 \cdot 10^{-7}$ m^2/s instead of $\kappa_{soil} = 3.22 \cdot 10^{-7}$ m^2/s. This can be explained by the error-plots of figure 4.2, where is shown that the model is robust to small changes in diffusivity.

[1] Analytical solutions were obtained by dr. Van der Linden (co-supervisor of this project), which are going to be published as peer-reviewed paper soon (2021). His results are used here to benchmark our numerical results, with permission of dr. Van der Linden and prof. Van de Wiel.

With the numerically calculated temperature profile $T(z,t)$, step 5 can be executed, and $G(0.05\text{m},t)$ can be diagnosed directly for a range of λ's. The associated measurements are corrected with the factor Φ of equation 3.2. The error is calculated with equation 3.17. Figure 4.5 shows the error e_G versus the inserted λ_{soil} underneath a bare and grass surface for the period 07/07/2006-17/07/2006. The optimal parameters are $\lambda_{soil} = 1.04\ \text{Wm}^{-1}\text{K}^{-1}$ for bare soil and $\lambda_{soil} = 0.57\ \text{Wm}^{-1}\text{K}^{-1}$ for grass-covered soil. The errors respectively are $e_G = 14.6\ \text{Wm}^{-2}$ and $e_G = 1.7\ \text{Wm}^{-2}$.

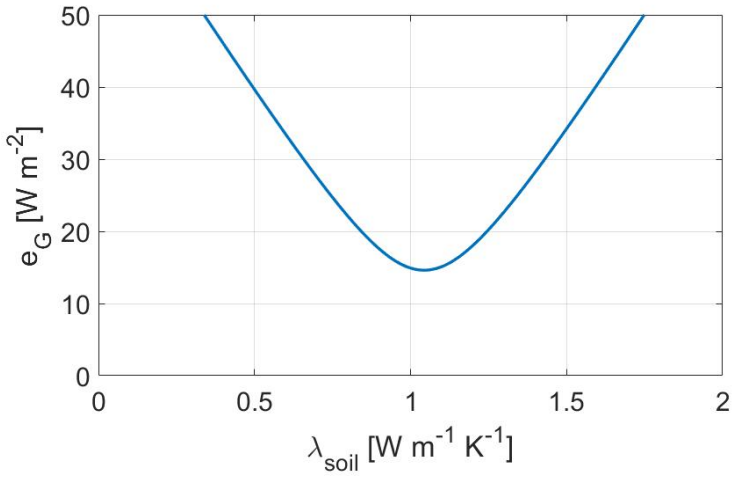

(a) Minimum is located at $\lambda_{soil} = 1.04\ \text{Wm}^{-1}\text{K}^{-1}$ and $e_G = 14.6\ \text{Wm}^{-2}$.

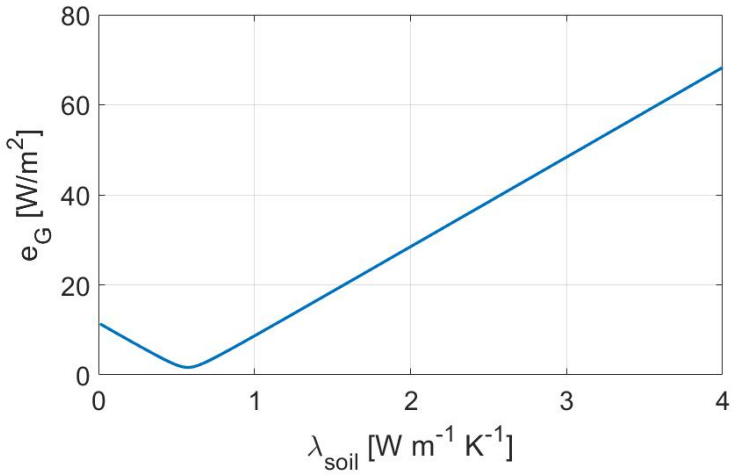

(b) Minimum is located at $\lambda_{soil} = 0.57\ \text{Wm}^{-1}\text{K}^{-1}$ and $e_G = 1.7\ \text{Wm}^{-2}$.

Figure 4.5: The error e_G is plotted against the inserted value for λ_{soil} for bare soil (a) and grass-covered soil (b) for the period 07/07/2006-17/07/2007.

In contrast to the results above, where the minima in the error functions of e_T versus κ were not sharply defined (the plots were 'L'-shaped), the minima in figure 4.5 are. This means that the model is indeed sensitive to any deviation of λ. Furthermore, we see again that the overall error in the bare soil is larger than that of the grass-covered soil. Again this can be explained because the extrema in G are greater for bare soil than for grass-covered soil, as can be seen in figure 4.6. Like mentioned before, the result could be generalized by scaling with the maximum amplitudes over bare soil and grass-covered soil respectively.

Figure 4.6 shows the measured and modeled soil heat flux at z = 5cm depth using the optimized value λ_{soil} (that is, the lowest value for e_G). The measured soil heat flux is corrected for instrumental shape and properties (see equation 3.2). Again, the model seems fairly accurate. For grass-covered soil (4.6b), the observational data and modeled heat flux nearly coincide. For bare soil (4.6a), some of the peaks are not modeled that well. We have modeled the heat flux with a constant value for λ. As we will investigate in section 4.2, it is possible that λ itself is variable over time due to e.g. temporal changes in soil moisture. One could even consider varying λ over shorter time intervals. However, the smaller the time interval, the larger the influence of noise of the measurements. The minimum time interval in this research to optimize κ and λ is therefore an individual day.

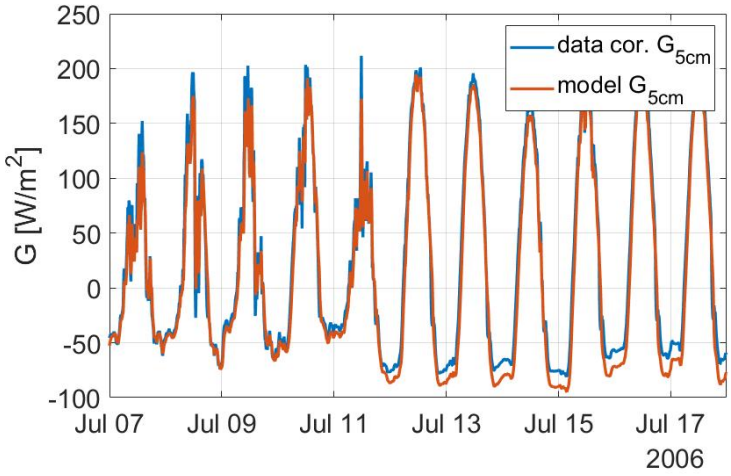

(a) λ_{soil} = 1.04 Wm^{-1}K^{-1} and e_G = 14.6 Wm^{-2}.

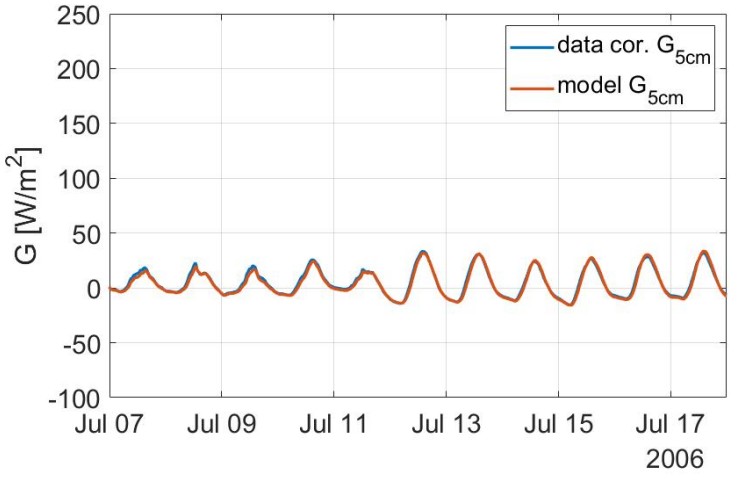

(b) λ_{soil} = 0.57 Wm^{-1}K^{-1} and e_G = 1.7 Wm^{-2}.

Figure 4.6: The measured (and corrected) and modeled soil heat flux at 5cm depth for bare soil (a) and grass-covered soil (b).

To illustrate that κ and λ may vary due to variation in soil moisture, another 11-days period, 25/08/2006-04/09/2006, is analyzed in the same way. These periods are chosen because they show a difference in soil moisture. The mean moisture of the periods are $\overline{\Theta}_{P_1}$ = 0.13 and $\overline{\Theta}_{P_2}$ = 0.24, where P_1 denotes the first period and P_2 the second period. Table 4.1 presents the periods and the optimized parameters of the bare and grass-covered soil. The resulting figures for period 2 can be found in appendix A.

Table 4.1 shows that κ barely changes in the two different periods, only 11% (soil underneath bare surface) and 2% (underneath grass surface). This agrees with figure 2.2, where κ does not increase or decrease considerably with soil moisture. Furthermore, figure 4.2 shows that the model is not sensitive to any deviations

Table 4.1: In this table, the optimized parameters κ and λ are presented for two periods. The parameters are given for both bare and grass-covered soils.

Period	Dates	κ_{bare} [m^2/s]	λ_{bare} [$Wm^{-1}K^{-1}$]	κ_{grass} [m^2/s]	λ_{grass} [$Wm^{-1}K^{-1}$]
1	7-17 July 2006	$3.37 \cdot 10^{-7}$	1.04	$3.22 \cdot 10^{-7}$	0.57
2	25 Aug-4 Sept 2006	$3.74 \cdot 10^{-7}$	1.20	$3.29 \cdot 10^{-7}$	1.01

in κ. λ on the other hand increases with 15% (bare surface) and 77% (grass surface) from the dry to the wet period. Indeed figure 2.2 shows that λ should increase with increasing moisture and figure 4.5 shows that the model is sensitive to deviations in λ.

4.2. Thermal parameters and soil moisture

The preliminary analysis above indicated that we expect the most variation in λ compared to soil moisture. Next, we are going to quantity this dependence in more detail i.e. we aim to monitor $\lambda = f(\Theta)$. To this end, we use the numerical scheme as described in section 3.3 to find the optimal values for the parameters. In section 4.1 we applied the model on two periods of 11 days. In this section, we will optimize the parameters for separate days from 01/05/2006 to 31/10/2006. For each day, the diffusivity and conductivity are determined. Figure 4.7 shows the daily determined optimal parameters κ_{opt} (figure (a)) and λ_{opt} (figure (b)) versus time. In the same figures, the soil moisture at 5cm depth is plotted as to visualize a possible relation. Please note that the soil moisture is measured beneath grass-covered soil only. Therefore, in this part of the project, the model is applied to grass-covered soil only (and not to soil covered by bare surface).

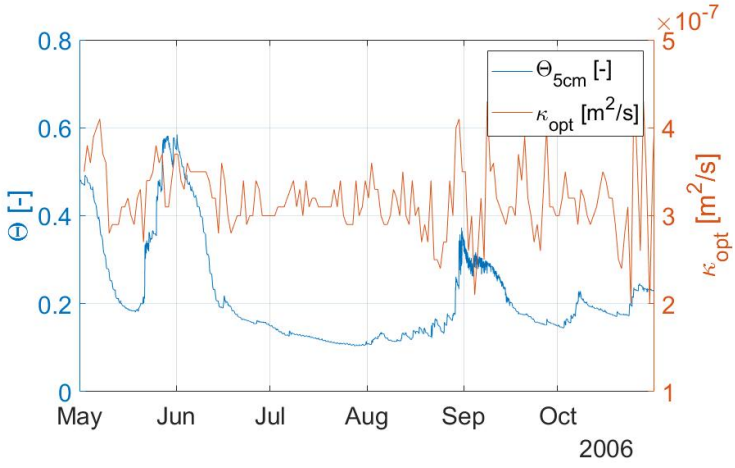

(a)

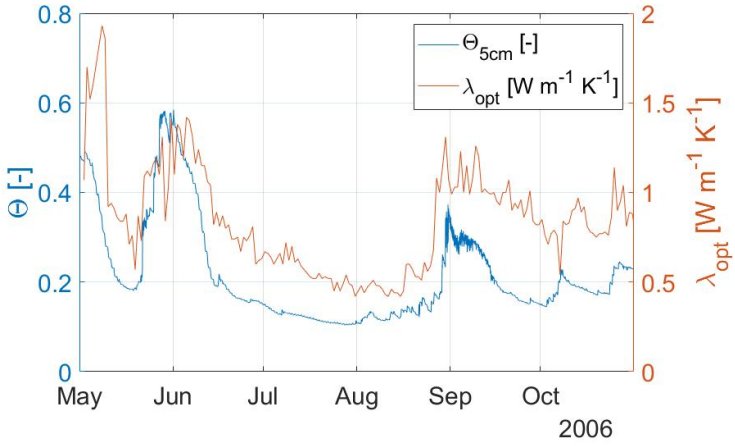

(b)

Figure 4.7: In this figure, the optimal values for the parameters κ and λ per day are plotted in red versus time. The soil moisture at 5cm depth is plotted in blue. The diffusivity and soil moisture do not show a clear correlation, but the conductivity and soil moisture do.

Figure 4.7a does not show a clear relation between diffusivity and moisture. This is in line with the conceptual view in figure 2.2, where it was shown that moisture dependencies in both thermal conductivity and thermal heat capacity largely cancel each other, such that the diffusivity is almost independent of soil moisture content. Figure 4.7b however does show a clear relation between conductivity and soil moisture. The peaks in soil moisture at the beginning of May, beginning of June, and beginning of September, are accompanied by peaks of conductivity. This is supported by the relation shown in figure 2.2, where λ goes to a maximum if Θ goes to a maximum.

The relations between moisture and thermal parameters can be visualized more clearly by making scatter plots between Θ and the conductivity or diffusivity. This is done in figure 4.8. The red data points denote days where the fits are relatively inaccurate (i.e. $e_T > 0.1$°C or $e_G > 5$ Wm^{-2}).

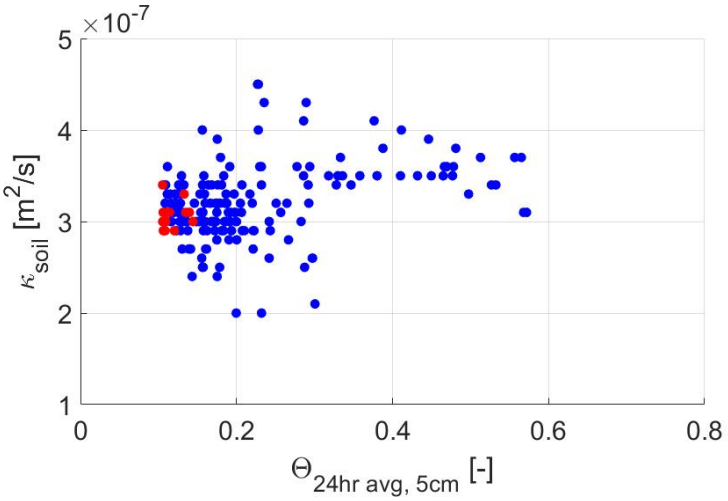

(a) Red data points denote days where $e_T > 0.1$ °C.

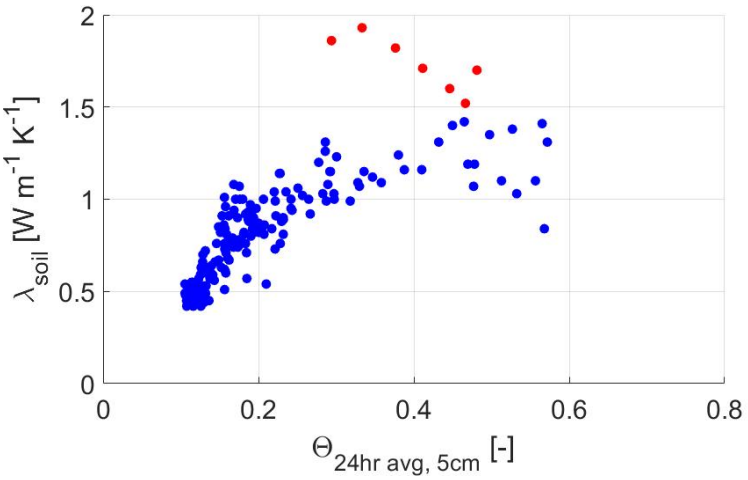

(b) Red data points denote days where $e_G > 5$ Wm^{-2}.

Figure 4.8: This figure shows the daily determined thermal diffusivity (a) and conductivity (b) versus the daily mean soil moisture measured at 5cm. The red data points denote days where the errors e_T and e_G are relatively large.

For the diffusivity, the expectation is that for very low values of Θ the diffusivity increases for increasing moisture, after which the diffusivity hits a maximum and starts decreasing (see figure 2.2). Because there is no numerical data given in figure 2.2, it is not possible to say where the maximum is. In this research, we deal with 'heavy basin clay' [7]. The curve in figure 2.2 for clay barely shows any increase or decrease. It is hard to relate figure 4.8a to figure 2.2. It seems that the diffusivity increases over moisture for small values for moisture, after which it reaches a 'ceiling'. The values for κ for values of $\Theta < 0.3$ however are too scattered to make this claim founded and to draw a definite conclusion. The data in this region should be acquired more precisely. Furthermore, it is recommendable to calculate κ over a larger region of Θ to accurately derive a numerical relation.

Secondly, 4.7b shows the relation between λ and Θ. Theoretically, it is expected that the conductivity would rapidly increase (see explanation section 2.2) and then level off. If the red data points are omitted, which seems reasonable because the fit at those days is poor ($e_G > 5$ Wm^{-2}), the theoretically expected behavior seems to be present in our data as well. Below we elaborate on the quantitative relation.

In figure 4.9, we show a yellow fit curve through the blue data points of 4.7b. The fit has the form $y = ax^b + c$ and is optimized by Matlab (minimizing least squared deviations). In the equation, x denotes soil moisture Θ [-] and y denotes conductivity λ [$Wm^{-1}K^{-1}$]. There is no theoretical foundation behind the equation of the fit. It is purely based on the description that λ increases for increasing moisture but that the increase slows down. Figure 2.2 does for example not show if the curves go through the origin or if λ reaches a constant maximum.

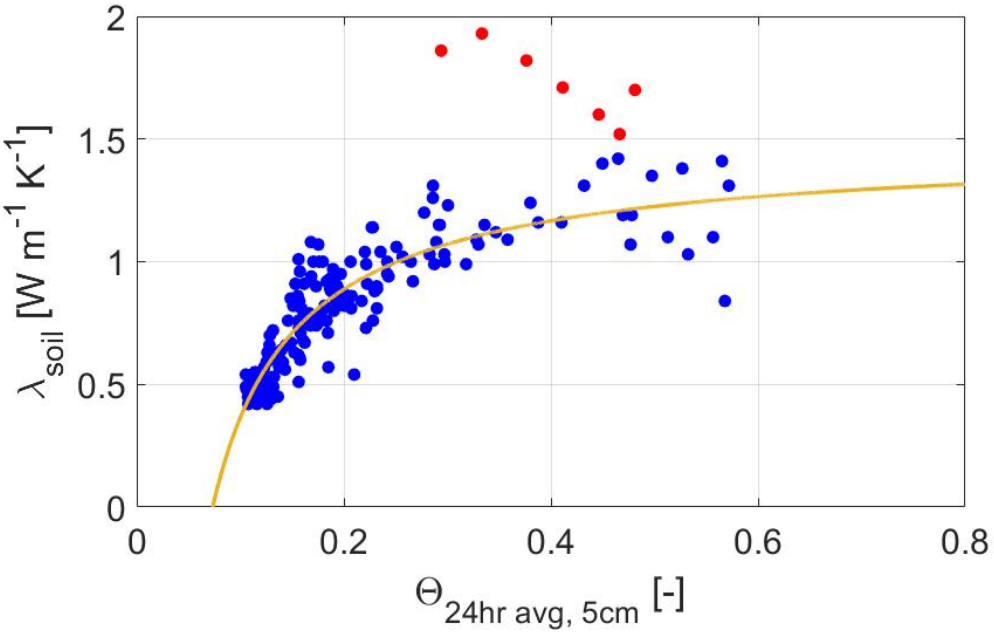

Figure 4.9: This figure is the same as figure 4.8b with an added fit through the blue data points of the form $y = ax^b + c$. The results of the fit are $a = -0.14\ Wm^{-1}K^{-1}$, $b = -0.91$ and $c = 1.49\ Wm^{-1}K^{-1}$, with a root-mean-square error (RMSE) of $0.11Wm^{-1}K^{-1}$.

The results of the fit are $a = -0.14\ Wm^{-1}K^{-1}$, $b = -0.91$ and $c = 1.49\ Wm^{-1}K^{-1}$, with a root-mean-square error (RMSE) of $0.11Wm^{-1}K^{-1}$. Next, we consider limit behaviour. If soil moisture goes to infinity, λ goes to $c = 1.49\ Wm^{-1}K^{-1}$ according to the fit, which seems reasonable. However, if $\Theta < (\frac{-c}{a})^{\frac{1}{b}} = 0.07$, λ would be negative, which is not allowed. Therefore we recommend not to use this empirical formulation for values of Θ lower than 0.1.

The current research was done on clay soil in a moderate climate. As to assess the generality of the results, we also analyzed silty clay loam soil in a semi-arid environment. However, in view of brevity, those results are given in appendix B.

4.3. Modeling heat transfer in soil and vegetation: a two-layer system

The third goal in this research was to apply the numerical scheme to a two-layer system, which consists of a vegetation layer (z from -0.10m to 0m) and a soil layer (z from 0m to 0.10m) which are both assumed homogeneous in itself, to calculate the temperature $T(z,t)$. The procedure is about the same as in section 4.1, however, the thermal diffusivity now has two distinct values: For the vegetation layer, where $-0.1\text{m} < z < 0\text{m}$, $\kappa = \kappa_{veg}$, and for the soil layer, where $0\text{m} < z < 0.1\text{m}$, $\kappa = \kappa_{soil}$. Again, we select a period of data, as can be seen in figure 4.10, where the radiation temperature T_{IRT} and the soil temperatures T_{5cm} and T_{10cm} (5cm and 10cm underneath the grass) are given. The radiation temperature is calculated out of the longwave radiation via equation 3.1.

In [6] was shown that in soil the amplitude of the temperature decreases with depth. Furthermore, there is a phase shift compared to the surface temperature. Both aspects are visible in figure 4.10 for the soil temperatures, but also for the radiation temperature T_{IRT}. This motivates to model the grass layer (similarly to soil) as a homogeneous layer, but with different thermal properties: hence, the two-layer model. Note also the insulating effect of the vegetation: The distance from T_{IRT} to T_{5cm} is only 15cm, but the temperature amplitude already has decreased considerably.

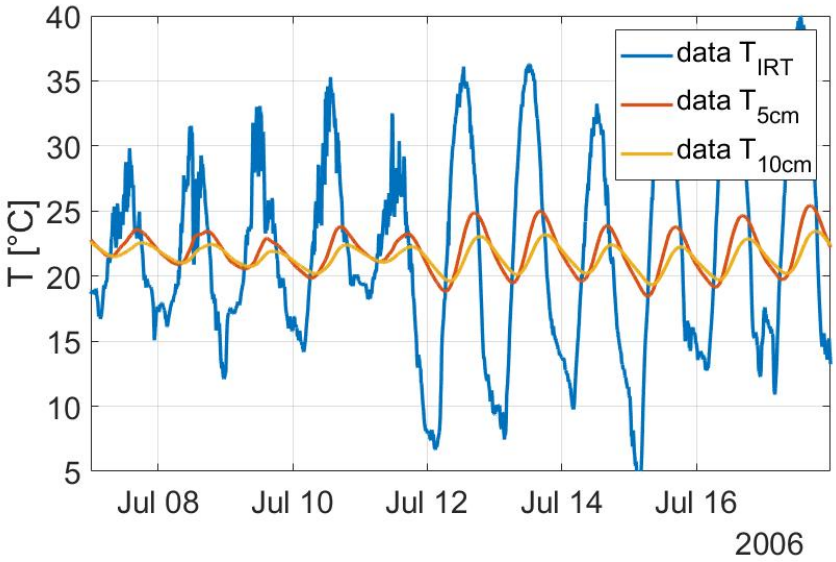

Figure 4.10: In the figure, the temperature data for depths of 5 and 10cm are given for the period 07/07/2006-17/07/2006. The soil is covered with grass. The radiation temperature (IRT) is calculated out of the longwave radiation via equation 3.1.

The domain is created from $z = -0.10\text{m}$ up until 0.10m in steps of $\Delta z = 0.01\text{m}$ and a range is created for possible values of κ_{veg} and κ_{soil}. As explained in section 3.3, the mean temperatures for 2006 are subtracted from the data. Because $\overline{T_{IRT}^{2006}} = 11.1\ ^\circ\text{C}$ and $\overline{T_{5cm}^{2006}} = \overline{T_{10cm}^{2006}} = 12.0\ ^\circ\text{C}$, this results in a raise of the T_{IRT} of 0.9°C with respect to the soil temperatures. The boundary conditions are the radiation temperature T_{IRT} and the temperature at 10cm depth T_{10cm} interpolated to the 30s interval. The initial condition is a spline interpolation with $\Delta z = 1\text{cm}$ over the temperatures T_{IRT}, T_{5cm} and T_{10cm}.

The third step is to calculate $T(z,t)$ for each combination of κ_{soil} and κ_{veg}. The associated error can then be calculated via equation 3.16, where the error is a function of κ and κ is a function of κ_{veg} and κ_{soil}, or $e_T(\kappa) = e_T(\kappa_{veg}, \kappa_{soil})$. The temperature predicted by the numerical model at 5cm depth is compared to the observed temperature. Note that the mean temperature $\overline{T^{2006}_{5cm}}$ is added back to the modeled temperature before calculating the error. We can visualize e_T as an error landscape, as can be seen in 3D (a) or in 2D top view (b) in figure 4.11.

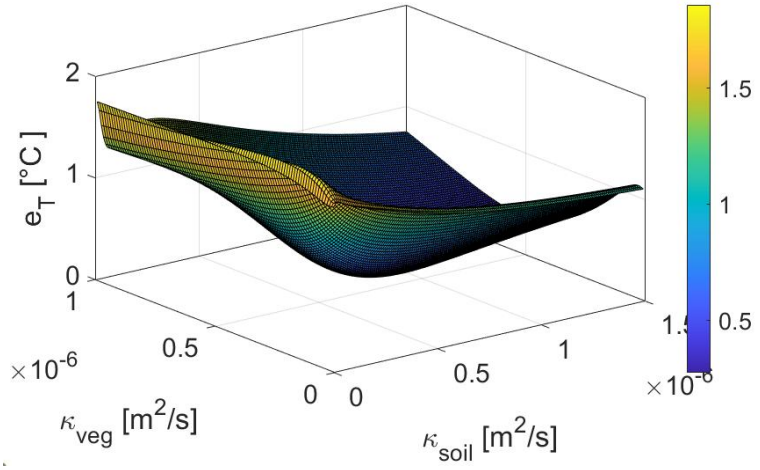

(a)

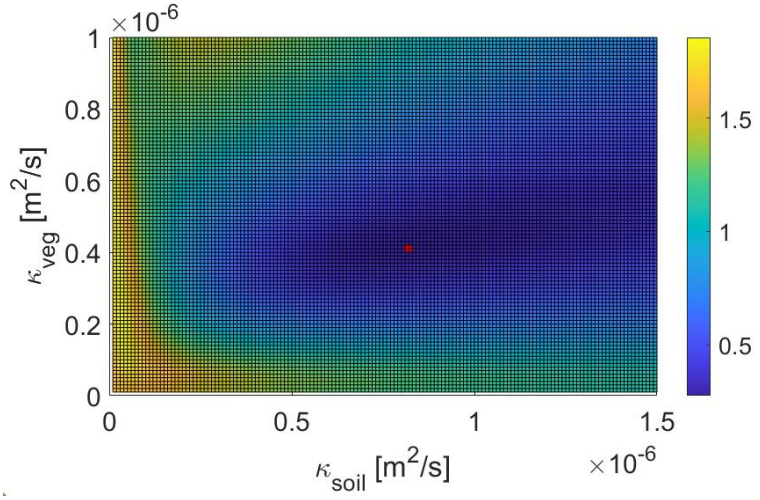

(b)

Figure 4.11: The error landscape of the two-layer method in 3D (a) and in 2D top view (b), where the error is plotted as a function of diffusivity of soil (κ_{soil}) and vegetation (κ_{veg}) for the period 07/07/2006-17/07/2006. The global minimum is found at $\kappa_{soil} = 8.2 \cdot 10^{-7}$ m^2/s and $\kappa_{veg} = 4.1 \cdot 10^{-7}$ m^2/s, where $e_T = 0.27$ °C, and is denoted by the red dot.

The global minimum in the error landscape is denoted by a red dot, as can be seen in the 2D top view. It is located at $\kappa_{soil} = 8.2 \cdot 10^{-7}$ m^2/s and $\kappa_{veg} = 4.1 \cdot 10^{-7}$ m^2/s, where $e_T = 0.27$ °. We note that the found soil diffusivity κ_{soil} is greater than found in section 4.1 ($\kappa_{soil} = 3.22 \cdot 10^{-7}$ m^2/s), which will be further discussed in section 4.4. The dark blue area covers a large area, which means that the error landscape around the minimum is relatively 'flat' and so the model is robust to parameter changes.

Again, the results are compared to that of the harmonic model. The resulting figures are however not shown here, since the harmonic model has a slightly different approach for two layers. The harmonic model optimizes the diffusivity parameter throughout the soil layer first, whereafter it extends to the grass layer and optimizes the grass diffusivity parameter. Figure 4.4b already showed that $\kappa_{soil} = 3.0 \cdot 10^{-7}$ m^2/s for the one-layer model of the grass-covered soil, and so this is also the value for the soil diffusivity in the harmonic two-layer model. This is far away from the numerical result of $\kappa_{soil} = 8.2 \cdot 10^{-7}$ m^2/s (figure 4.11). The value for the diffusivity of the grass however is rather large for the harmonic model compared to the numerical model: $\kappa_{veg} = 13.3 \cdot 10^{-7}$ m^2/s and $\kappa_{veg} = 4.1 \cdot 10^{-7}$ m^2/s. To be able to compare the results of the two models, the harmonic model could be optimized for the two parameters κ_{soil} and κ_{veg} simultaneously[2].

Figure 4.12 shows the measured temperature and the modeled temperature at $z = 5$cm depth for the optimal values for $\kappa_{soil} = 8.2 \cdot 10^{-7}$ m^2/s and $\kappa_{veg} = 4.1 \cdot 10^{-7}$ m^2/s. Note again that the measured temperature plotted in blue almost coincides with the modeled temperature in red. This result is nontrivial, if one considers the enormous change of the signal between the boundary of the system T_{IRT} and the temperature prediction at 5cm in the soil (see the enormous change in amplitude in figure 4.10).

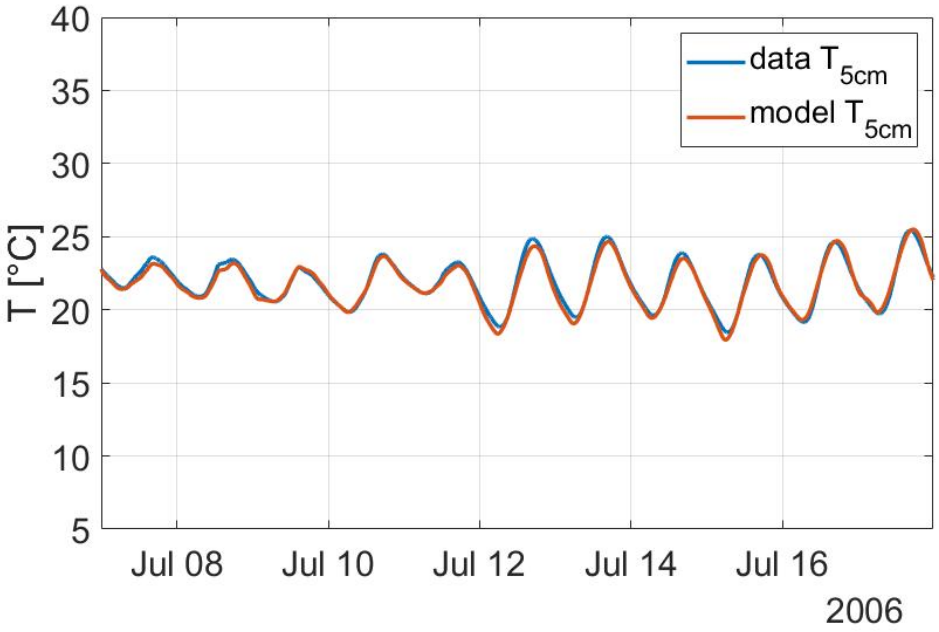

Figure 4.12: The measured and modeled temperature at 5cm depth for grass-covered soil. The modeled temperature is calculated with the two-layer model. Note that the blue data line almost coincides with the red model line.

The two-layer system seems to work surprisingly well (in view of its simplicity) and the blue and red lines almost coincide. Compared to figure 4.3b however, the blue data line in figure 4.12 is more visible. This means that the residuals are greater, which is supported by the difference in error: $e_T = 0.08$ °C for the one-layer model versus $e_T = 0.27$ °C for the two-layer model. One explanation is that if we compare figure 4.1b with figure 4.10 we see that the radiation temperature T_{IRT} has greater extrema than the soil temperatures, so the upper boundary condition has a larger influence. Another argument is that whereas the one-layer model only uses one assumed homogeneous layer, the two-layer model uses two. Vegetation (grass in this case) is not as homogeneous as soil, as it contains more air and is easier deformable (for example by wind). A last logical explanation for the increase in e_T is that the error for the two-layer model is evaluated at 5cm, whereas for one-layer is evaluated at 10cm, which by nature has a smaller amplitude overall.

[2]Analytical solutions were obtained by dr. Van der Linden (co-supervisor of this project), which are going to be published as peer-reviewed paper soon (2021). His results are used here to benchmark our numerical results, with permission of dr. Van der Linden and prof. Van de Wiel.

With the numerically calculated temperature profile $T(z,t)$, step 5 can be executed, where $G(0.05\text{m},t)$ is calculated for a range of λ's with equation 3.18. The error is calculated with equation 3.17, in which the corrected heat flux G^{cor} is the measured heat flux corrected with the factor Φ (equation 3.2). The error e_G is plotted against the conductivity λ_{soil} in figure 4.13a. The optimal parameter is $\lambda_{opt} = 0.62\text{Wm}^{-1}\text{K}^{-1}$ with an error of $e_G = 4.49\text{Wm}^{-2}$. The optimal modeled heat flux is plotted in 4.13b together with the measured heat flux, which is corrected for instrumental shape.

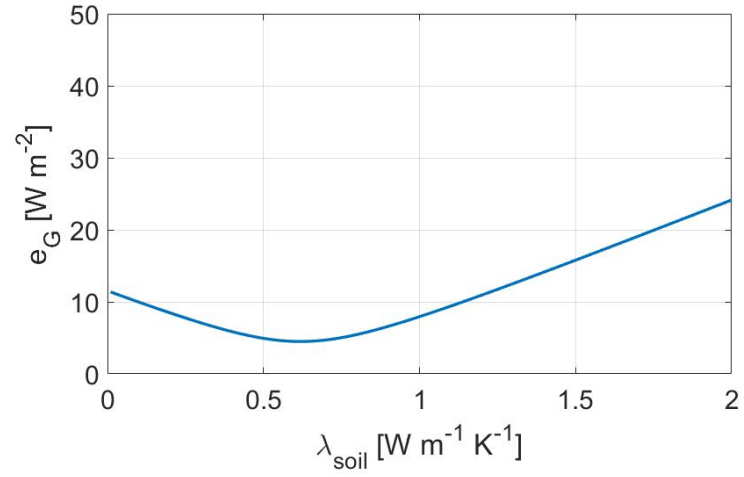

(a)

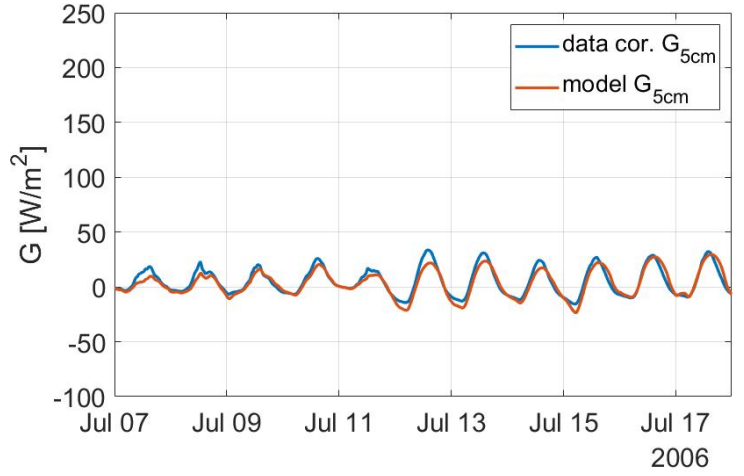

(b)

Figure 4.13: Figure (a) show the error function of G. The minimum is located at $\lambda_{opt} = 0.62\text{Wm}^{-1}\text{K}^{-1}$ with an error of $e_G = 4.49\text{Wm}^{-2}$. Figure (b) shows the modeled heat flux and the measured data, which is corrected for instrumental shape.

Similar to section 4.1, a second period is analyzed to compare the results, which is again from 25/08/2006-04/09/2006. The period is analyzed with the two-layer model in the same way as period 1 and the results can be found in appendix A. The results are summarized in table 4.2.

Table 4.2: In this table, the optimized parameters κ_{soil}, κ_{veg} and λ_{soil} are presented for two periods. These parameters are found by using the two-layer method.

Period	Dates	κ_{soil} [m^2/s]	κ_{veg} [m^2/s]	λ_{soil} Wm^{-1}K^{-1}
1	7-17 July 2006	$8.2\cdot10^{-7}$	$4.1\cdot10^{-7}$	0.62
2	25 Aug-4 Sept 2006	$10.0\cdot10^{-7}$	$2.1\cdot10^{-7}$	1.13

4.4. Discussion and implications of results

As can be seen in figures 4.1 and 4.6, the extrema of temperature and heat flux are larger for the bare soil than for the grass-covered soil, which can best be described as 'the insulating effect of grass': During the day, less heat is stored into grass-covered soil, with the consequence that during the night, less heat is stored back into the atmosphere. This insight was also discussed in [5] by Maarten Kruis, who provided the example that this phenomenon leads to a mean difference in heat flux at the soil interface of about 20Wm^{-2} during the night for the year 2003. This is an important argument in removing grass from orchards in the battle against fruit frost.

The number of 20Wm^{-2} was calculated by using two thermal parameters: diffusivity κ and conductivity λ. In our research, the goal was to develop a numerical model to investigate the robustness of these parameters. Figure 4.3 shows that the numerical model works and that it can be used to analyze the thermal parameters.

As can be seen in figure 4.2, the error-plot e_T versus κ has a sort of an 'L'-shape: a large gradient at the left of the minimum and a small gradient at the right. The optimal diffusivity for a grass-covered soil for the shown period is $\kappa_{soil} = 3.22 \cdot 10^{-7}$ m^2/s with an error of $e_T = 0.08$ °C. For example, let's consider a value of $\kappa_{soil} = 8.2 \cdot 10^{-7}$ m^2/s, as was calculated with the two-layer model. The error of the one-layer model would increase to $e_T = 0.25$ °C (figure 4.2), which still is fairly accurate. We conclude that the value of κ_{soil} does not matter that much for the outcome of this numerical model and it is a robust parameter. This is a reason why no clear relation between daily diffusivity and soil moisture was obtained: For low values of soil moisture, κ spreads out over a large range, which can be explained by the flatness of the error plots.

The error function of e_G versus the conductivity λ shows a 'U-shape' dependency, as can be seen in figure 4.5. This means that the model is sensitive to chosen values of λ. Therefore, the model is a good tool to visualize the relation between daily conductivity and soil moisture (and vice versa). In figure 4.9 this is depicted along with a mathematical fit function to the data. The fit cannot be regarded to be universal for the full moisture range, as it would result in negative values for λ for low values of soil moisture. Nevertheless, it gives an impression of how the relation could look like in the region $0.1 < \Theta < 0.6$. To ameliorate the quality of the fit, more data should be acquired over a broader range of Θ.

The third goal was to model the temperature and heat flux throughout a two-layer model, consisting of grass and soil, which was successful (figures 4.12 and 4.13). It was observed that the 'optimal' κ_{soil} value for this soil in this two-layer system differed from the optimized value in the one-layer system. This can be explained by the robustness of the results to parameter variation (insensitivity to κ_{soil} in general). Another explanation for the difference in κ_{soil} for the one- and two-layer model is that soil just under the surface is less homogeneous than further away from the surface. In this shallow soil, more organic material is present (think of roots of vegetation or (parts of) small animals). Also, it is not completely smooth at the surface but rather a bit bumpy. Moreover, weather - such as rain or wind - has the largest influence on the shallow soil.

Finally, some crude assumptions were made in this study to simplify reality:

- The depth of the sensors is constant.
- The soil remains in place (although it may be influenced by root growth, rainfall, and animal movement).
- Grass remains in place (although it deforms for example by wind) and is of a constant 10cm height (although it grows and it is mowed).

We, therefore, recommend that in future work, those assumptions are re-assessed, so that additional improvements or model refinements can be made to describe reality.

5

Conclusion

Here, the research questions will be answered, and some important discussion points and recommendations are provided.

1. Can we reproduce the temperature and soil heat flux profiles throughout a soil layer with a numerical model and are the solutions accurate in comparison with a harmonic benchmark model?

The numerical model accurately reproduced the temperature and heat flux profiles, both for bare soil and grass-covered soil. The profiles were first modeled over two 11-days periods with constant thermal parameters, after which they were modeled for individual days, with daily varying parameter values. The difference between the two periods showed that the diffusivity parameter was not influenced (much) by soil moisture, but that conductivity was. The results were very similar to those of the analytical, harmonic model. This demonstrates that the developed numerical model can be used to find and analyze the thermal parameters.

2. Can we use the numerical model to estimate the thermal parameters of the soil?
   (a) How robust are these parameters?
   (b) How do these parameters relate to soil moisture?

The numerical model was used to estimate the thermal parameters of the soil by minimizing the difference between the modeled temperature and heat flux profiles and the measured profiles. The modeled temperature proved not to be very sensitive to changes in diffusivity, so diffusivity is a robust parameter. In contrast, the model performance showed to be sensitive to the choice of the conductivity parameters.

An advantage of the numerical model compared to the harmonic model is that the numerical model is more flexible and is also suited to model short periods (individual days) subject to time-dependent parameter changes. The daily determined parameters could therefore be related to the daily mean soil moisture. The diffusivity does not show a clear dependency on soil moisture. The conductivity on the other hand does show a clear dependency, from which a quantitative relation was described in the investigated region of moisture values covered by the observations. We recommend that in future research the investigated moisture range is broadened as to further generalize the results.

3. Can we reproduce the temperature and soil heat flux profiles throughout a two-layer system of vegetation and soil?

The numerical model for the one-layer soil domain was extended with a vegetation layer. Again, the temperature and heat flux profiles were modeled and showed good agreement with the measurements. The optimal value for the diffusivity of the soil layer was however higher than when the model was applied to a single grass-covered soil layer for the same period. If we would insert this value in the one-layer model, the root-mean-square error would increase from e_T = 0.08 °C to e_T = 0.25 °C, which still is fairly accurate. We conclude again that the model is not very sensitive to the value of the diffusivity. Another reason for the increase in diffusivity could be that the assumption of homogeneity is not justified for the grass layer and the direct layer beneath it, as the composition of shallow soil is influenced greatly by weather, plants, and animals. We recommend that in future research, the homogeneity of the soil is assessed at different depths, to further improve the model results.

We conclude that the research questions have been answered and that this numerical model can be used to study heat transfer in the vegetation-soil continuum. We used the model to demonstrate the influence of grass-cover or bare surface on heat transfer into or out of the soil. It would be interesting to see how the removal of vegetation would play out in practice: The temperature of the orchard would increase during the night, but on the other hand, it would be impractical for a farmer to remove all its grass (think for example of heavy machinery that is not able to drive over mud). It would be interesting to set up a study to compare the yields of orchards in grass-covered and bare surface environments. Furthermore, we used the model to quantitatively describe the relation between soil moisture and soil heat conductivity in the investigated region of moisture. We recommend broadening this region as to generalize the relation.

A

Extra figures second period

A.1. One-layer model

In this section of the appendix, period 2 (25/08/2006-04/09/2006) is analysed for the one-layer model. The calculated parameters are presented in table 4.1. Figure A.1 shows the data for T_{5cm}, T_{10cm}, and T_{20cm} for bare soil and grass soil for the period 25/08/2006-04/09/2006. Compared to figure 4.1, the y-axis is shifted 10 degrees downwards.

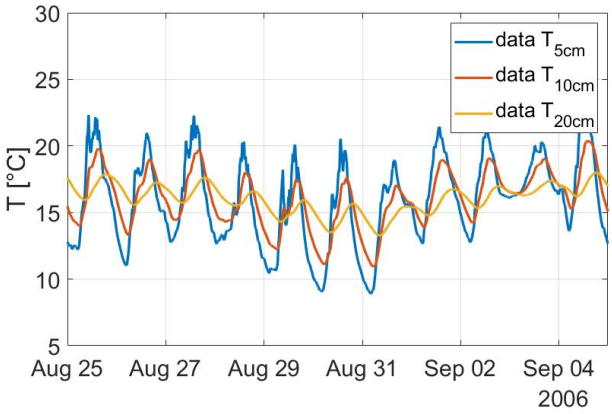

(a)

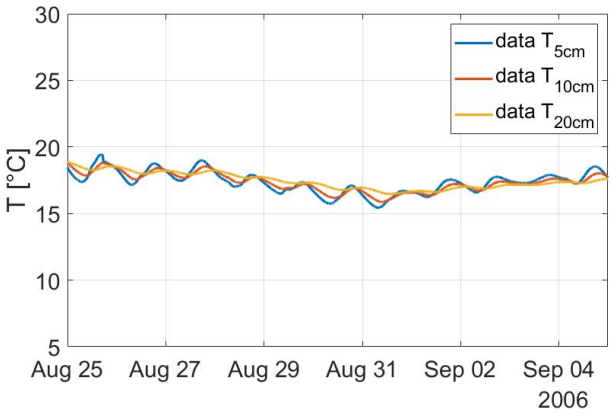

(b)

Figure A.1: In the figure, the temperature data for depths of 5, 10 and 20cm are given for the period 25/08/2006-04/09/2006. Figure (a) represents a bare soil, figure (b) represents a grass soil.

Figure A.2 shows the calculated error e_T plotted against the inserted κ_{soil}, for both the bare and grass soil. The optimal parameters are $\kappa_{soil} = 3.74 \cdot 10^{-7}$ m^2/s for bare soil and $\kappa_{soil} = 3.29 \cdot 10^{-7}$ m^2/s for grass soil. The minimum errors are then respectively $e_T = 0.11$ °C and $e_T = 0.05$ °C.

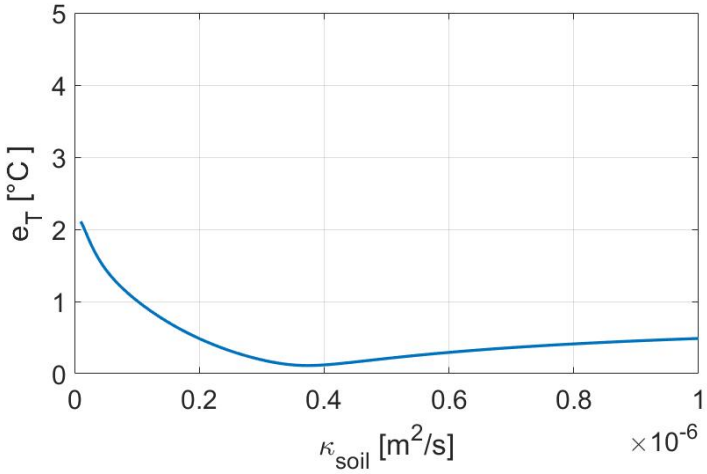

(a) Minimum is located at $\kappa_{soil} = 3.74 \cdot 10^{-7}$ m^2/s and $e_T = 0.11$ °C.

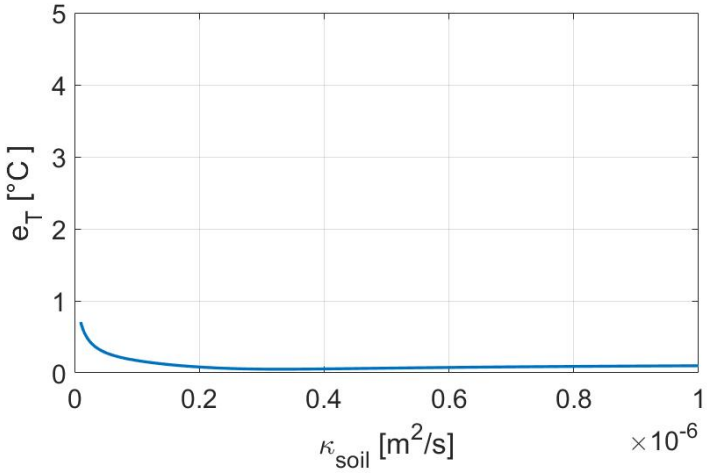

(b) Minimum is located at $\kappa_{soil} = 3.29 \cdot 10^{-7}$ m^2/s and $e_T = 0.05$ °C.

Figure A.2: The error e_T is plotted against κ_{soil} for bare soil (a) and grass soil (b) for the period 25/08/2006-04/09/2006.

Figure A.3 shows the measured temperature and the modeled temperature at z = 10cm depth for the optimal value of κ_{soil}. Compared to figure 4.3, the y-axis is shifted 10 degrees downwards.

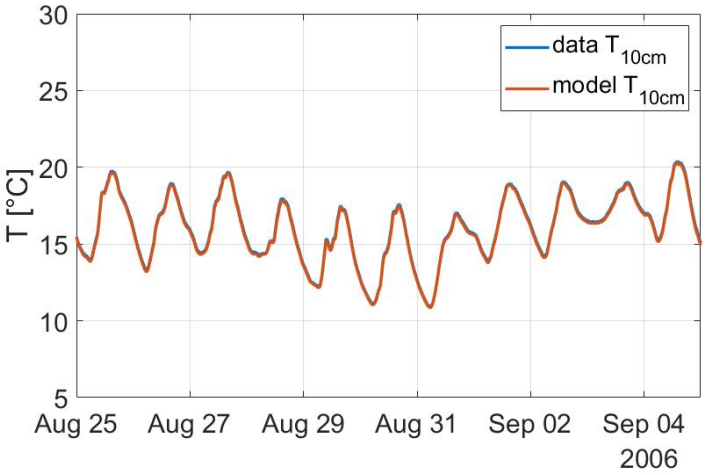

(a) $\kappa_{soil} = 3.74 \cdot 10^{-7}$ m^2/s and $e_T = 0.11$ °C.

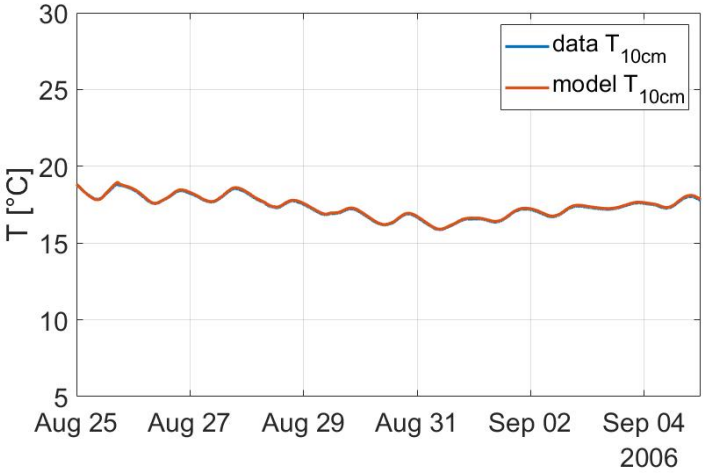

(b) $\kappa_{soil} = 3.29 \cdot 10^{-7}$ m^2/s and $e_T = 0.05$ °C.

Figure A.3: The measured and modeled temperature at 10 cm depth for bare soil (a) and grass soil (b).

Figure A.4 shows the error e_G versus the inserted λ_{soil} for bare soil and grass soil for period 2. The optimal parameters are $\lambda_{soil} = 1.20$ Wm^{-1}K^{-1} for bare soil and $\lambda_{soil} = 1.01$ Wm^{-1}K^{-1} for grass soil. The errors respectively are $e_G = 7.33$ Wm^{-2} and $e_G = 2.26$ Wm^{-2}.

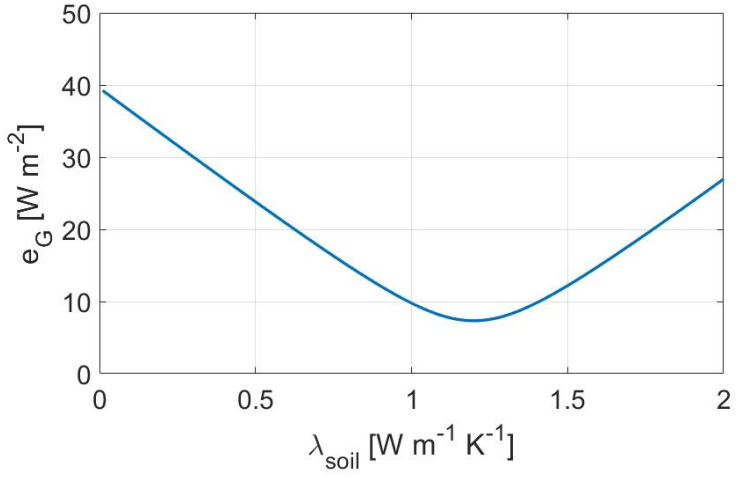

(a) Minimum is located at $\lambda_{soil} = 1.20$ Wm^{-1}K^{-1} and $e_G = 7.33$ Wm^{-2}.

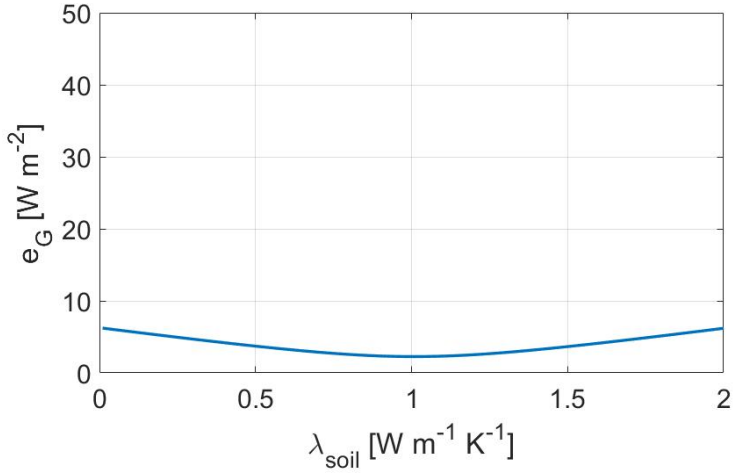

(b) Minimum is located at $\lambda_{soil} = 1.01$ Wm^{-1}K^{-1} and $e_G = 2.26$ Wm^{-2}.

Figure A.4: The error e_G is plotted against the inserted value of λ_{soil} for bare soil (a) and grass soil (b) for the period 25/08/2006-04/09/2006.

Figure A.5 shows the measured and modeled soil heat flux at $z = 5$cm depth for the optimal values of λ_{soil}. The measured soil heat flux is also corrected for instrumental shape.

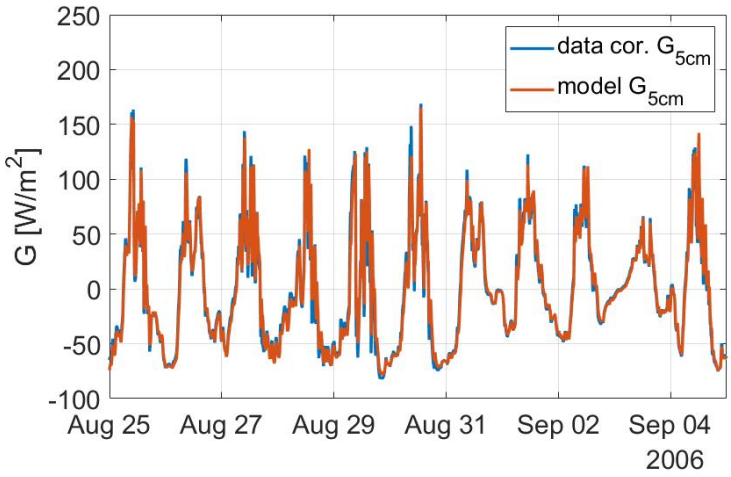

(a) $\lambda_{soil} = 1.20\ \mathrm{Wm^{-1}K^{-1}}$ and $e_G = 7.33\ \mathrm{Wm^{-2}}$.

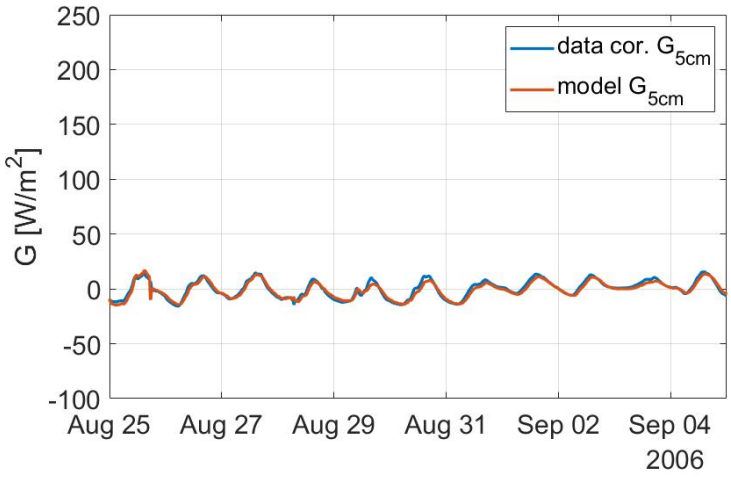

(b) $\lambda_{soil} = 1.01\ \mathrm{Wm^{-1}K^{-1}}$ and $e_G = 2.26\ \mathrm{Wm^{-2}}$.

Figure A.5: The measured (and corrected) and modeled soil heat flux at 5cm depth for bare soil (a) and grass soil (b).

A.2. Two-layer model

In this section of the appendix, period 2 (25/08/2006-04/09/2006) is analysed for the two-layer model. The calculated parameters are presented in table 4.2. Figure A.6 shows the error landscape e_T as a function of κ_{veg} and κ_{soil} for period 2. The minimum error of $e_T = 0.15$ °C is located at $\kappa_{soil} = 10.0 \cdot 10^{-7}$ m^2/s and $\kappa_{veg} = 2.1 \cdot 10^{-7}$ m^2/s.

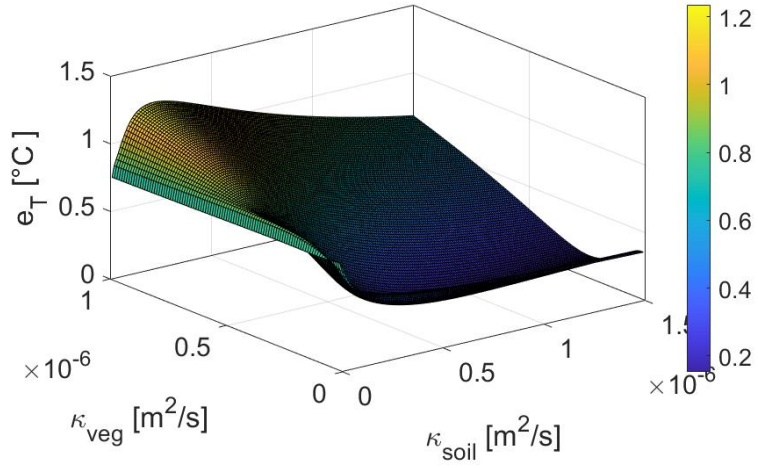

(a)

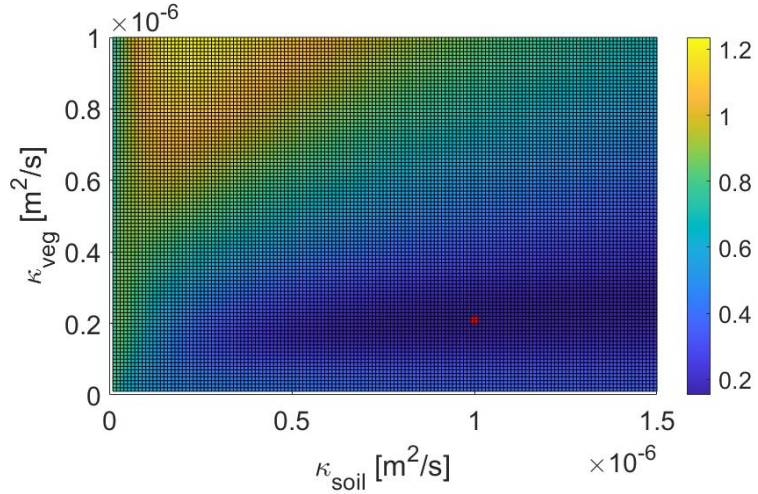

(b)

Figure A.6: The error landscape of the two-layer method in 3D (a) and in 2D top view (b), where the error is plotted as a function of diffusivity of soil (κ_{soil}) and vegetation (κ_{veg}) for the period 25/08/2006-04/09/2006. The global minimum is found at $\kappa_{soil} = 10.0 \cdot 10^{-7}$ m^2/s and $\kappa_{veg} = 2.1 \cdot 10^{-7}$ m^2/s, where $e_T = 0.15$ °C, and is denoted by the red dot.

Figure A.7a shows the radiation temperature T_{IRT} and the soil temperatures T_{5cm} and T_{10cm} for the grass soil for period 2. The radiation temperature is calculated out of the longwave radiation via equation 3.1. Figure A.7b shows the measured and modeled temperature at 5cm depth for the optimal parameters $\kappa_{soil} = 10.0 \cdot 10^{-7}$ m^2/s and $\kappa_{veg} = 2.1 \cdot 10^{-7}$ m^2/s.

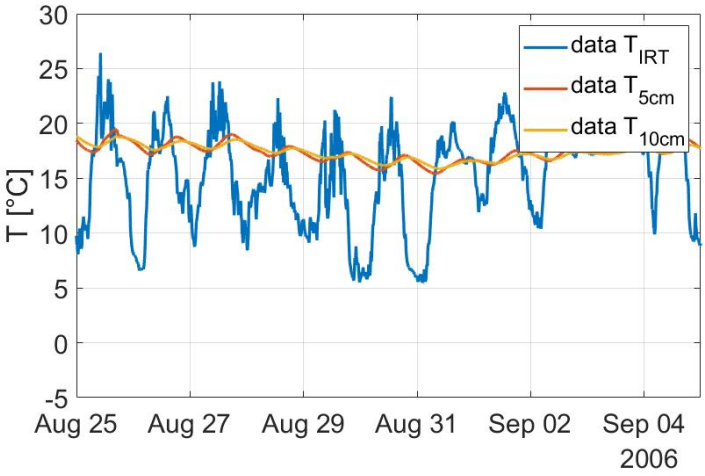

(a)

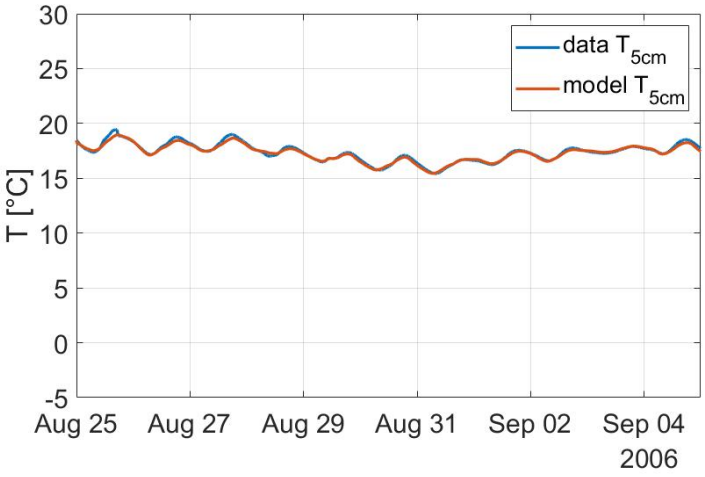

(b)

Figure A.7: Figure (a) shows the soil temperature data for depths of 5 and 10cm for period 2 for a grass soil. The radiation temperature is also given, calculated via equation 3.1. Figure (b) shows the modeled and measured temperature at 5cm depth for the optimal parameters $\kappa_{soil} = 10.0 \cdot 10^{-7}$ m^2/s and $\kappa_{veg} = 2.1 \cdot 10^{-7}$ m^2/s.

Lastly, step 5 is executed, where $G(0.05\text{m}, t)$ is calculated for a range of λ's from the calculated temperature profile $T(z,t)$. The error function is depicted in figure A.8a, where e_G is plotted against the inserted λ. The optimal parameter is $\lambda_{opt} = 1.13\text{Wm}^{-1}\text{K}^{-1}$ with an error of $e_G = 3.81\text{Wm}^{-2}$. The modeled heat flux is plotted in figure A.8b for the optimal conductivity, together with the measured heat flux corrected for instrumental shape.

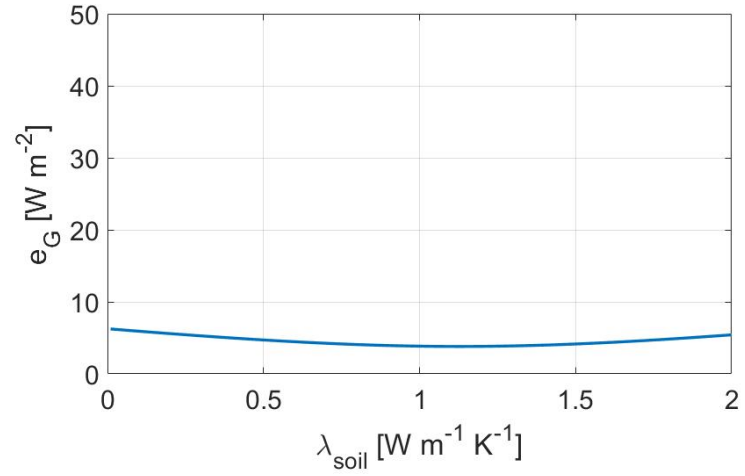

(a)

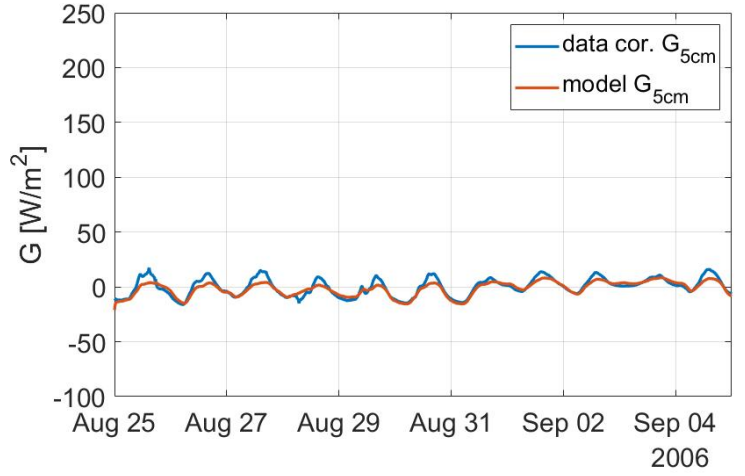

(b)

Figure A.8: Figure (a) show the error function of G. The minimum is located at $\lambda_{opt} = 1.13\text{Wm}^{-1}\text{K}^{-1}$ with an error of $e_G = 3.81\text{Wm}^{-2}$. Figure (b) shows the modeled heat flux and the measured data, which is corrected for instrumental shape.

B

Data set Texas

In this appendix, the Texas data is analyzed in the same way as the Haarweg data in section 4.2. Figure B.1 shows the daily determined optimal parameters κ_{opt} (figure (a)) and λ_{opt} (figure (b)) versus time. In the same figures, the soil moisture at 8cm depth is plotted to visualize a possible relation. We see that there are gaps in the data set of the soil moisture. These gaps are filled by linear interpolation as an intermediate step in the model, but do not play a role in the final Θ, κ- and Θ, λ-plots.

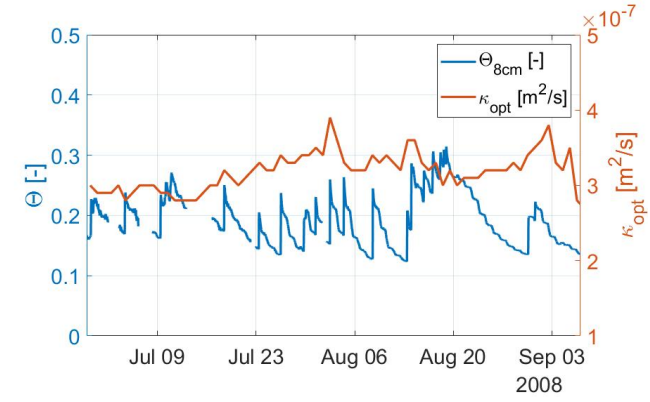

(a)

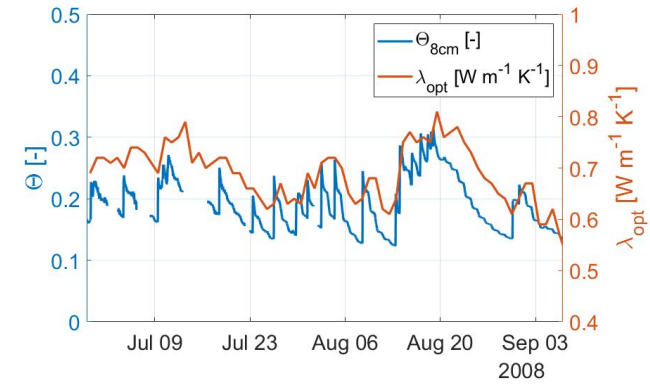

(b)

Figure B.1: In this figure, the optimal values for the parameters κ and λ are plotted in red versus time. The soil moisture at 8 cm depth is plotted in blue. Similarly to figure 4.7, the diffusivity does not show a clear relation with soil moisture whereas the conductivity does.

Figure B.1 shows that there is no clear relation between the peaks in diffusivity and soil moisture, but there is a clear relation between the peaks in conductivity and moisture, which is the same result as we had in section 4.2.

Again, we visualize the relations more clearly by making a Θ,κ- and a Θ,λ-plot, which are presented in figure B.2. Note that the range of soil moisture is smaller compared to figure 4.8. The range of soil moisture of the Haarweg data is approximately 0.1 to 0.6, whereas the range of soil moisture of the Texas data is approximately 0.1 to 0.3. The red data points are the days with soil moisture data gaps. The yellow line denotes a fit of the form $y = ax^b + c$ through the blue data points and is optimized by Matlab.

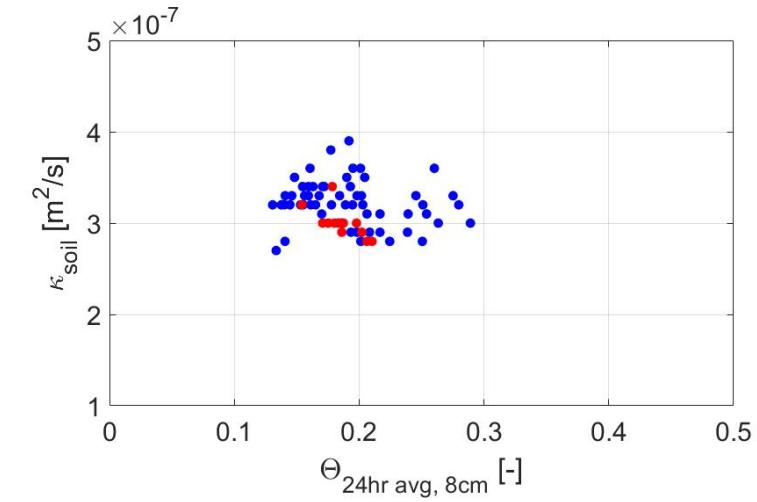

(a)

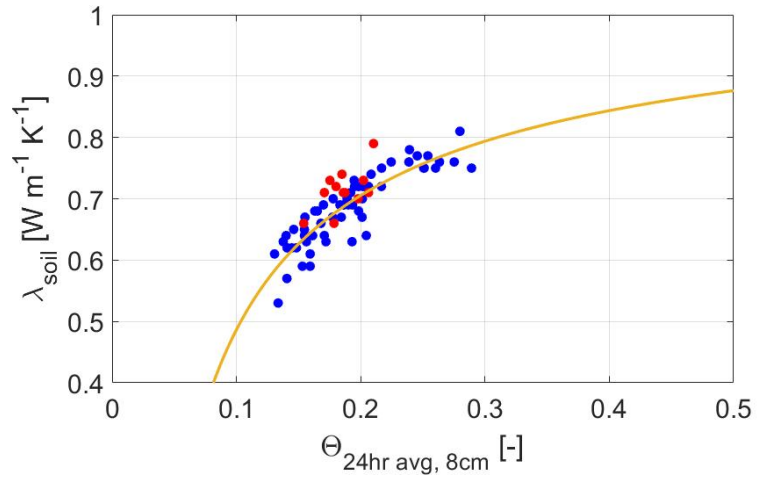

(b)

Figure B.2: This figure shows the daily determined thermal diffusivity (a) and conductivity (b) versus the daily mean soil moisture measured at 8cm. The red data points denote days where there is a soil moisture data gap. The results of the fit are $a = -0.13\ \mathrm{Wm^{-1}K^{-1}}$, $b = -0.66$ and $c = 1.08\ \mathrm{Wm^{-1}K^{-1}}$, with a root-mean-square error (RMSE) of $0.03\mathrm{Wm^{-1}K^{-1}}$.

The range of soil moisture is smaller than that of the Haarweg data set, but the relation between the conductivity λ and soil moisture Θ is visible. The conductivity increases for increasing moisture, but the increase slows down. The results of the fit are $a = -0.13\ \mathrm{Wm^{-1}K^{-1}}$, $b = -0.66$ and $c = 1.08\ \mathrm{Wm^{-1}K^{-1}}$, with a root-mean-square error (RMSE) of $0.03\mathrm{Wm^{-1}K^{-1}}$. If soil moisture goes to infinity, λ goes to $c = 1.08\ \mathrm{Wm^{-1}K^{-1}}$ according to the fit, which seems reasonable. However, if $\Theta < (\frac{-c}{a})^{\frac{1}{b}} = 0.04$, λ would be negative, which is not allowed. The diffusivity again does not show a clear relation with the moisture.

Bibliography

[1] freepik, "Fresh spring green grass with soil isolated on white background," May 2021. [Online]. Available: https://www.freepik.com/free-photo/fresh-spring-green-grass-with-soil-isolated-white-background_1007830.htm

[2] J. Rodrigo, "Spring frosts in deciduous fruit trees—morphological damage and flower hardiness," Scientia Horticulturae, vol. 85, no. 3, pp. 155–173, 2000.

[3] K. B. Perry, "Basics of frost and freeze protection for horticultural crops," HortTechnology, vol. 8, no. 1, pp. 10–15, 1998.

[4] Z.-F. Kijk, "Koud! de vignerons stoken fikkie in de wijngaarden," May 2021. [Online]. Available: https://kijkzuidfrankrijk.com/2021/04/08/koud-de-vignerons-stoken-fikkie-in-de-wijngaarden-filmpje/

[5] M. T. Kruis, "Towards a physical description of heat transfer over grass covered surfaces," Master's thesis, Delft University of Technology, 2020.

[6] A. F. Moene and J. C. Van Dam, Transport in the atmosphere-vegetation-soil continuum. Cambridge University Press, 2014.

[7] A. F. Jacobs, B. G. Heusinkveld, and A. A. Holtslag, "Towards closing the surface energy budget of a mid-latitude grassland," Boundary-layer meteorology, vol. 126, no. 1, pp. 125–136, 2008.

[8] A. F. Jacobs, B. G. Heusinkveld, and A. Holtslag, "Long-term record and analysis of soil temperatures and soil heat fluxes in a grassland area, the netherlands," Agricultural and Forest Meteorology, vol. 151, no. 7, pp. 774–780, 2011.

[9] O. K. Hartogensis, "Meteorological station haarweg 1974-2012: Data-set description." February 2015. [Online]. Available: http://www.met.wur.nl/haarwegdata

[10] Engineering ToolBox, "Emissivity coefficients common materials," May 2021. [Online]. Available: https://www.engineeringtoolbox.com/radiation-heat-emissivity-d_432.html

[11] Campbell Scientific, Inc., "Tdr100 time-domain reflectometer," April 2021. [Online]. Available: https://www.campbellsci.com/tdr100

[12] S. R. Evett, W. P. Kustas, P. H. Gowda, M. C. Anderson, J. H. Prueger, and T. A. Howell, "Overview of the bushland evapotranspiration and agricultural remote sensing experiment 2008 (bearex08): A field experiment evaluating methods for quantifying et at multiple scales," Advances in Water Resources, vol. 50, pp. 4–19, 2012.

[13] S. R. Evett, N. Agam, W. P. Kustas, P. D. Colaizzi, and R. C. Schwartz, "Soil profile method for soil thermal diffusivity, conductivity and heat flux: Comparison to soil heat flux plates," Advances in Water Resources, vol. 50, pp. 41–54, 2012.

[14] K. Hanjalić, S. Kenjeres, M. Tummers, and H. Jonker, Analysis and modelling of physical transport phenomena. VSSD, 2007.